FIELD MEASUREMENTS FOR ESTIMATING IMPACT LOADS ON GIRDER SUPPORTS FOR FERRY RAMPS

A Thesis

by

KIMBERLY ANN LYONS

Submitted to the Office of Graduate and Professional Studies of
Texas A&M University
in partial fulfillment of the requirements for the degree of

MASTER OF SCIENCE

Chair of Committee,	Gary Fry
Committee Members,	Peter Keating
	Alan Palazzolo
Head of Department,	Robin Autenrieth

May 2015

Major Subject: Civil Engineering

Copyright 2015 Kimberly Ann Lyons

ABSTRACT

In Port Aransas, TX, movable bridges, ferry ramps, are used to dock ferry boats and load vehicles on and off of the boats to cross the Corpus Christie, TX ship channel as part of State Highway 361. Fatigue cracks are present in several of the bearing assemblies that attach the ramps to the headwall at the ferry landing. The cracks were caused by axial forces in the main supporting beams of the ramps. Using strain gage instrumentation applied to the beams, estimates of the axial forces were obtained. A video camera was installed to allow the research team to distinguish between loading events caused by large or small ferry boats. The recorded data from the instrumentation was accessed remotely from Texas A&M University in College Station and analyzed using MatLAB, Mathematica, and Microsoft Excel. Load data was collected for several months. The information was used to develop recommendations for design loads to be used when the bearing assemblies are rebuilt. Results indicate that the exterior beams of the ramps experience the largest force values in compression caused by docking and thrusting of the ferry boats. The interior beams experience majority of the tension forces caused by vehicles crossing the ramps. To date, the largest force detected is 102.56 kips in compression.

DEDICATION

To Jesus Christ, my best friend and helper in all areas of my life.

ACKNOWLEDGEMENTS

I would like to thank my committee chair, Dr. Gary Fry for providing the opportunity to perform research at Texas A&M University. The knowledge and skills he has passed on to me will be very beneficial in work and life. Also, thank you to my committee members, Dr. Peter Keating and Dr. Alan Palazzolo, for their guidance and support throughout the course of this research.

Thanks also to the Center for Railway Research group for their assistance and encouragement. Special thanks to the following group members who have continuously been a part of my research: Austin Allard, Maysam Kiani, Johanna Posey, Lisa Rachal, Cynthia Ryan, and Amy White.

This project in Port Aransas, Texas was funded by the Texas Department of Transportation. Special thanks to the following Texas DOT employees for their help and support: Mike Hyzak, Howard Gillespie, Mark Hughes, and Bill Gunn. Other programs that should be acknowledged are the Zachry Department of Civil Engineering and the Texas Transportation Institute.

Finally, I want to thank my family and friends for always supporting me with love, joy, and motivation, especially my mother and father.

NOMENCLATURE

AASHTO	American Association of State Highway and Transportation Officials
CDF	cumulative distribution function
F	gage factor of strain gages
FHWA	Federal Highway Administration
GB	gigabytes
I	current
k	kips
NBIS	National Bridge Inspection Standards
R	resistance and nominal gage resistance
TX	Texas
TxDOT	Texas Department of Transportation
V	voltage
V_{ac}	output voltage
V_{in}	input voltage
x-bar	average
ΔR	change of resistance
ε	magnitude of mechanical strain
σ_{n-1}	standard deviation
ν	poisson's ratio

TABLE OF CONTENTS

Page

LIST OF FIGURES

Page

LIST OF TABLES

Page

CHAPTER I

INTRODUCTION AND BACKGROUND

1.1 Project Overview

In Port Aransas, TX, ferry boats are used to transport vehicles across the Corpus Christie Ship Channel on Highway 361. The ferry crossing is the shorter of two routes connecting Port Aransas, TX and Aransas Pass, TX. The longer route is 53 miles around the bay and through Corpus Christi, TX. The ramps that are used to load and unload the ferry boats are used simultaneously to dock the ferry boats. The ramps are essentially small movable bridges constructed from structural steel. They comprise of eleven longitudinal stringers each supported at the headwall by a hinged bearing assembly. A transverse beam supports the stringers at the other end of the ramp. This transverse beam is suspended by cables that are used to raise and lower the ramp for docking and undocking of the ferry boat. An electric motor, operated by members of the deck crew aboard the ferry boat, raises and lowers the ramp. The ramps resist forces caused by vehicles crossing them, by ferry boats docking and undocking, and by holding docked ferry boats in place in the presence of wind and waves. Axial forces in the stringers seem to be causing damage to the bearing assemblies at the headwall end of the ramps. The main objective of this study is to produce estimates of stringer axial loads using field measurements. After a sufficient time window of observations has been accumulated, recommendations for design loads can be developed using the data directly.

1.2 Bridge Inspection History

Civil engineering structures such as bridges and highways are subject to experiencing common deficiencies. Corrosion, fatigue cracking, collision damage, and heat damage are just a few of the many types of structural impairments occurring on infrastructure. Regular inspection and maintenance of highway bridges is required by the Federal Highway Administration (FHWA). The FHWA is responsible for ensuring that America's roads and highways continue to be among the safest and most technologically sound in the world (FHWA, 2012). The Texas Department of Transportation (TxDOT) follows the bridge design and inspection guidelines issued by the American Association of State Highway and Transportation Officials (AASHTO).

Regularly scheduled bridge inspections were not always the case in Federal highway history. Texas initiated an extensive road construction program following World War II causing a lot of emphasis on new construction and little emphasis to inspection and maintenance of current structures. It was in 1967 when bridge inspection and maintenance became a national concern for the United States. The Silver Bridge over the Ohio River at Point Pleasant, West Virginia, collapsed and resulted in 46 deaths. This catastrophe initiated a federal act for a national bridge inspection program to periodically and consistently perform bridge inspections. As a result of this program, the first National Bridge Inspection Standards (NBIS) were developed in 1971 (TxDOT, 2013).

According to the Bridge Inspection Manual adopted by TxDOT, bridge inspections are performed to ensure public safety and confidence in bridge structural capacity, protect

public investment, and effectively schedule maintenance and rehabilitation operations. These inspections provide a basis for repair, replacements and other improvements and ensure federal funding will remain available for bridge restoration and replacement. Typically, bridges are inspected every two years but more frequently depending on the condition of the bridge (TxDOT, 2013). There are five basic field inspections performed on bridges.

1. Initial Inspection – performed on new bridges.
2. Routine Inspections – regularly scheduled, usually every two years.
3. Event Driven Inspections (AASHTO Damage Inspections) – those performed as a result of collision, fire, flood, significant environmental changes, etc. Also known as Emergency Inspections and performed on an as-needed basis.
4. In-Depth Inspections – performed usually as a follow-up inspection to better identify deficiencies found in any of the above three types of inspection.
5. Special Inspections – performed to monitor a particular deficiency or changing condition.

Through routine inspections, the Port Aransas Ferry Ramps were identified for having cracks in the bearing connections, and TxDOT decided it would be beneficial to conduct an experiment to measure live loads impacting the bridges. The results from the field test would be used for administering design repairs or possible bridge redesign.

1.3 Movable Bridges

The ferry ramp at Port Aransas is a movable bridge. Defined by the FHWA's Bridge Inspector's Reference Manual (2012), movable bridges are constructed across designated "Navigable Waters of the United States", in accordance with "Permit Drawings" approved by the U.S. Coast Guard. Moveable bridges are powered by electric-mechanical or hydraulic mechanical drives. In the state of Texas, there are only 13 movable bridges among the 52,937 highways bridges (FHWA, 2014). Movable bridges are considered to be complex according to the NBIS. The NBIS requires identification of specialized inspection methods, and additional inspector training and experience required to inspect these complex bridges (FHWA, 2012).

The ferry ramps at Port Aransas are considered to be moveable lift bridges. Vertical lift bridges have a movable span with a fixed tower at each end. The span is supported by steel wire ropes that pass over pulleys atop the towers and connect to counterweights on the other side. The counterweights descend as the span ascends (FHWA, 2012). Some vertical lift bridges can go from being horizontal to completely vertical. That is not the case in Port Aransas. The ferry ramp only needs to be lifted an angle high enough for the ferry boats to be released. The ferry ramp is lowered for docking and raised for undocking. The ferry ramps at Port Aransas serve two purposes: it is a bridge for vehicles to drive across and a docking device that holds ferry boats in a stable position.

1.4 Strain Gages and Wheatstone Bridge Circuits

The instrumentation used to record live data from the movable bridge is strain gages. A strain gage is a device that experiences a change in electrical resistance in response to being strained mechanically. The change of resistance of a strain gage can be modeled by equation 1 and rearranged into equation 2.

$$\Delta R = \varepsilon F R \tag{1}$$

Rearranging terms yields the following.

$$\varepsilon = \frac{1}{F}\frac{\Delta R}{R} \tag{2}$$

In these equations, F is the gage factor of the strain gage, R is the nominal gage resistance, ε is the magnitude of mechanical strain, and ΔR is change in resistance due to mechanical strain. For this project, the values of F and R were 2.04 and 120 Ω respectively. For most strain gages, the gage factor tends to be around 2.0 and is provided by the manufacturer of the strain gage. When installed correctly, a strain gage experiences very nearly the same strain as the material to which it is bonded, and its resistance will change by a small amount. This small change in resistance can be detected and quantified most conveniently by incorporating the gage as one of the resistive elements in a Wheatstone bridge electrical circuit, an example of which is illustrated in Figure 1.

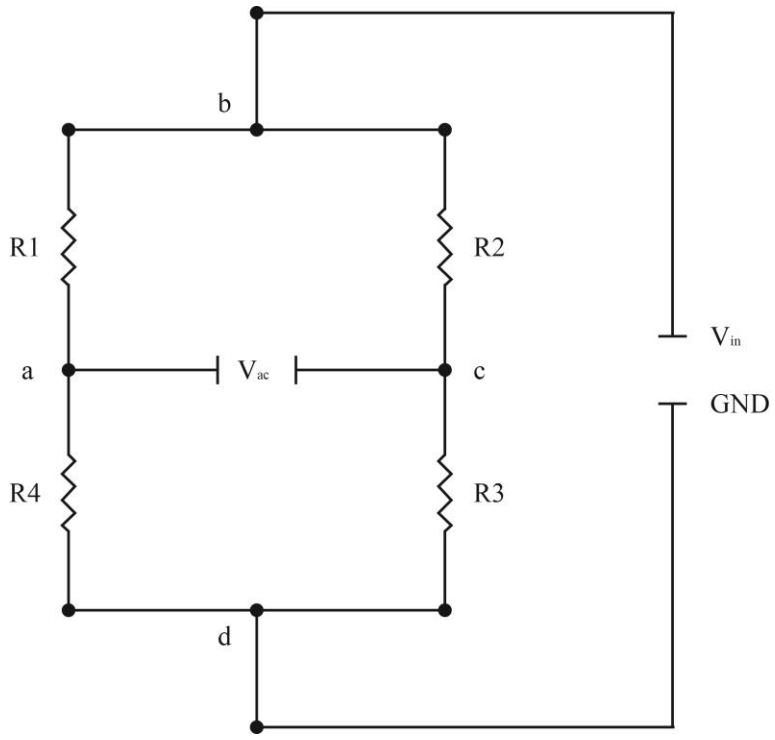

Figure 1 Wheatstone Bridge Circuit

As indicated in Figure 1, a Wheatstone bridge is an electrical circuit comprising of four resistors, an input voltage (V_{in}), and an output voltage (V_{ac}). A Wheatstone bridge can determine resistance, but it must be initially balanced to do so. When it is balanced, that means the output voltage (V_{ac}) is zero. The Wheatstone bridge can be balanced by a number of ways. One simple balancing technique is to have all resistors be equal. By having the Wheatstone bridge balanced, when an asymmetrical change in resistance occurs, then a voltage output reading across "ac" will be produced.

The derivation of the Wheatstone bridge equation starts with the simple equation known as Ohm's Law, equation 3, where V is voltage, I is current, and R is resistance.

$$V = IR \tag{3}$$

The output voltage across 'ac' of the Wheatstone bridge is the voltage 'ad' minus voltage 'cd'. Current can be further described as the input voltage divided by the resistors it passes through, resulting in:

$$\mathrm{V_{ac}} = \mathrm{V_{ad}} - \mathrm{V_{cd}} = \mathrm{I_L R_4} - \mathrm{I_R R_3} = \frac{\mathrm{V_{in} R_4}}{\mathrm{R_1 + R_4}} - \frac{\mathrm{V_{in} R_3}}{\mathrm{R_2 + R_3}} \tag{4}$$

Remove the input voltage from the parenthesis and the voltage across 'ac' is:

$$\mathrm{V_{ac}} = \mathrm{V_{in}} \left[\left(\frac{\mathrm{R_4}}{\mathrm{R_1 + R_4}} \right) - \left(\frac{\mathrm{R_3}}{\mathrm{R_2 + R_3}} \right) \right] \tag{5}$$

Change in resistance is what will produce an output voltage across 'ac', so is of interest in this project. By replacing every resistor with the initial resistance plus change in resistance produces the equation used in combining Wheatstone bridge with strain gages, equation 7.

$$\mathrm{R_i} = \mathrm{R_{io}} + \Delta \mathrm{R_i} = \mathrm{R} + \Delta \mathrm{R_i} \tag{6}$$

$$\mathrm{V_{ac}} = \mathrm{V_{in}} \left[\left(\frac{\mathrm{R} + \Delta \mathrm{R_4}}{2\mathrm{R} + \Delta \mathrm{R_4} + \Delta \mathrm{R_1}} \right) - \left(\frac{\mathrm{R} + \Delta \mathrm{R_3}}{2\mathrm{R} + \Delta \mathrm{R_3} + \Delta \mathrm{R_2}} \right) \right] \tag{7}$$

By inserting equation 1 from strain gages into equation 7 results in a relationship between voltage across 'ac' and strain gages through change in resistance giving equation 8. This is how the Wheatstone bridge is used as a tool with strain gages.

$$\mathrm{V_{ac}} = \mathrm{V_{in}} \left[\left(\frac{1 + \mathrm{F}\varepsilon_4}{2 + \mathrm{F}\varepsilon_4 + \mathrm{F}\varepsilon_1} \right) - \left(\frac{1 + \mathrm{F}\varepsilon_3}{2 + \mathrm{F}\varepsilon_3 + \mathrm{F}\varepsilon_2} \right) \right] \tag{8}$$

1.5 Strain Gage Placement

Longitudinal forces applied to the ferry ramp are the main concern for this project. Longitudinal forces can occur from docking and undocking of the ferries, self-weight, thrust from the boat's engine, wind, and waves. The strain gages used for this project were arranged in a full bridge configuration to maximize the output readings caused by longitudinal forces. Each of the 11 stringers has four gages attached to it and wired to form a full bridge Wheatstone bridge circuit with two gages on each side of the stringer, as can be seen in Figure 2.

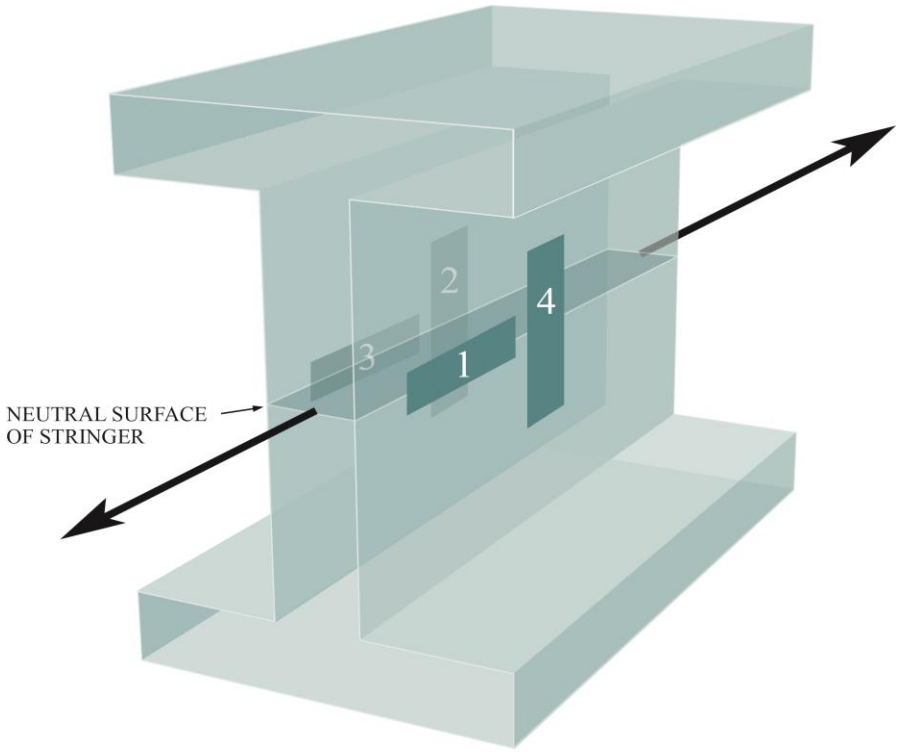

Figure 2 Full bridge, axial load configuration on I-beam

The strain gages are placed mid-depth at the neutral axes of each stringer. The strain gages are arranged to maximize Wheatstone bridge output. The axial strain of the stringer is defined as ε. The strain in gages 1 and 3 are represented by ε because they are the longitudinal strain gages, whereas gages 2 and 4 are equal to $-\nu(\varepsilon)$ because they are subjected to the transverse strain caused by axial load in the stringer.

Forces due to bending are not a concern in this study, and this arrangement of strain gages cancels strain caused by bending moments. The voltage readings that would normally come from temperature changes are also canceled (or compensated). As temperature increases, the steel stringers will expand thus causing an axial strain in the stringer. A similar effect, but opposite in sense, occurs when the temperature decreases, the steel will contract causing an axial strain. By having the strain gages placed as shown in Figure 2, the gages will experience a symmetrical change in resistance from temperature, thus remaining balanced and producing no voltage output.

Long cabling is another factor that can affect the output data. The cabling connecting the strain gages to the data box in Port Aransas is roughly longer than 25 feet. The chosen 10 volts of input for each of the strain gage circuits is transmitted through these cables, and the voltage measurements are sent back to the data systems from the strain gages through these cables. Due to the length the data must travel, there is a possibility for voltage loss because of the electrical resistance of the cable. This is similar to the concept of head loss with water pipes. To accommodate for the cable length, the data acquisition system monitors the voltage potential at the strain gages and increases the

excitation voltage at the supply end of each cable to ensure that 10 volts is provided at the instrument end.

CHAPTER II

EXPERIMENTAL PROCEDURES

2.1 Installation of Strain Gages

The steps below were used in the procedure to install the strain gages on ramp 1 in Port Aransas. It should be noted that the research team attached each strain gage to their cables in the laboratory, and verified proper functioning of the instruments prior to field installation.

1. Maintenance personnel removed the grated panels positioned over the end of the bridge to allow an opening in the ramps for access to the stringers.
2. Cable bundles were untangled, laid out, and organized by stringer.
3. An outline of the area needed to be ground away was marked on both sides of every stringer with a sharpie and accurately measured stencil.
4. A grinder was used to remove the paint and galvanization leaving exposed metal where the strain gages must attach.
5. The neutral axes were marked, on each side of every stringer, with a sharpie, stencil, and level to display where the strain gages must be attached.
6. Strain gages were attached to the stringers with a small welder.
7. Several coats of zinc spray paint were sprayed over all the installed strain gages to prevent rust and damage to the sensors followed by a rust resistant primer and top coat paint system.
8. Cables were routed to a weather protected box where the data acquisition system was kept. Zip-ties were used to route the cabling along the edge of the wall.

9. The cables were connected to the data acquisition system that was connected to the laptop.
10. The DASYLab program was brought up on the laptop to begin sensor readings and offset the gages.

Figures 3 through 8 provide visual representation of the installation day.

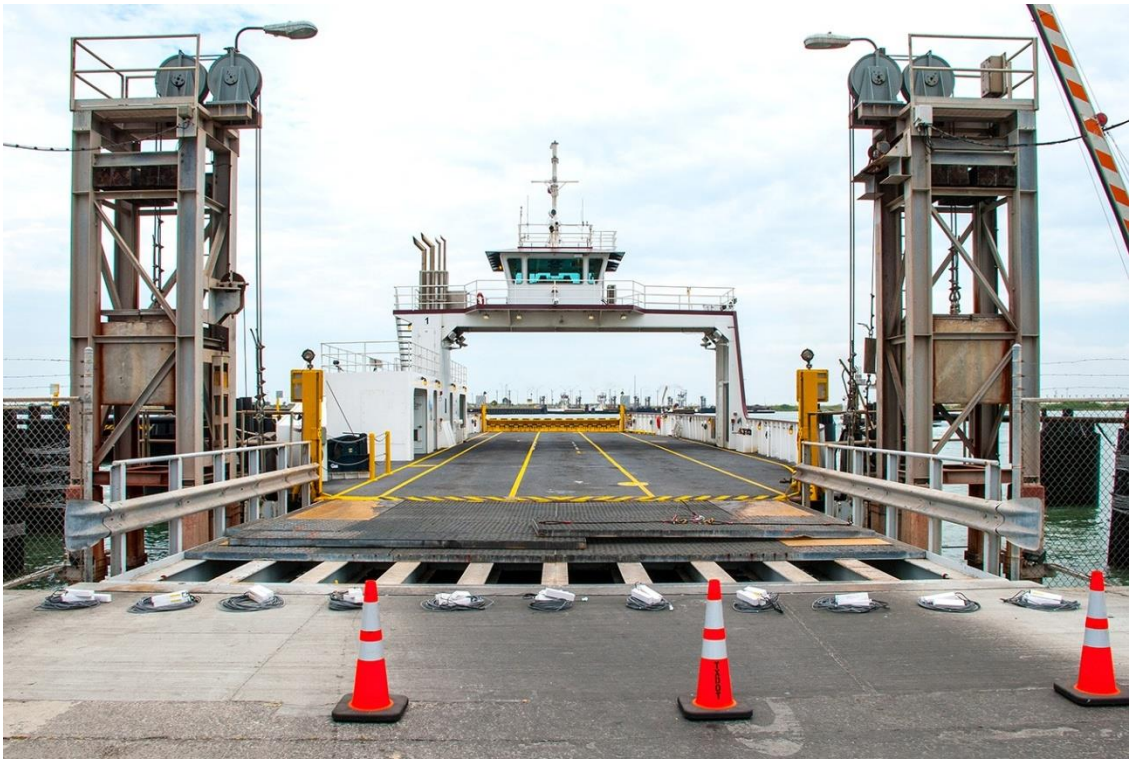

Figure 3 Ramp 1 at the Port Aransas, TX ferry facility with grates removed

Figure 4 Using a template, the exact locations for each strain gage were marked

Figure 5 A grinder was used to remove the paint, primer, and zinc galvanization

A **B**

Figure 6 Strain gages after installation: (A) east face of stringers, (B) west face

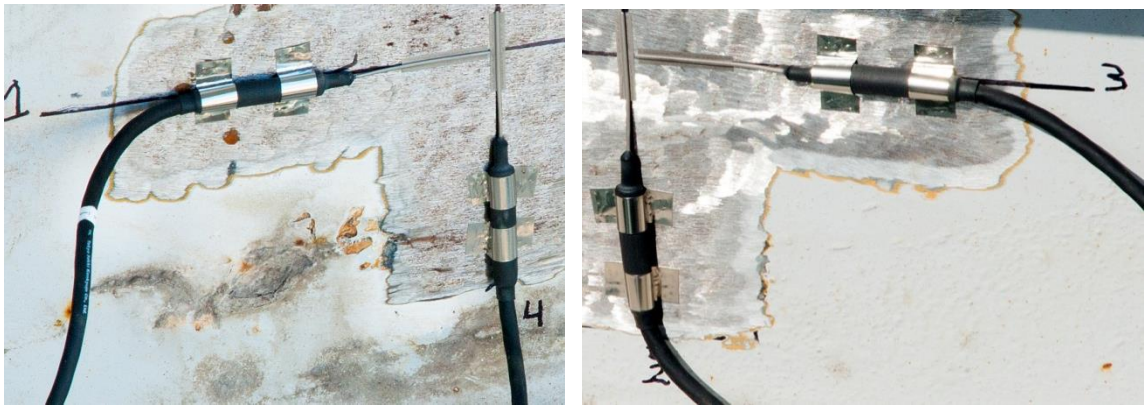

A **B**

Figure 7 Numbers correspond to resistor element positions in the Wheatstone bridge circuit: (A) 1 and 4 are on the east face, (B) 2 and 3 are on the west face

A **B**

Figure 8 A rust resistant paint system was applied to protect against corrosion: (A) zinc spray paint and rust resistant primer, (B) top coat of paint

2.2 Installation of Video Camera

The ferry crossing in Port Aransas uses big and small boats to transport cars across the channel. Different sizes of boats can cause different magnitudes in forces. A video camera was installed at the project site to specify small or big boats with load events. The camera is a 2 megapixel night vision dome model that records surveillance from detecting motion. The camera was routed to the IP-Pro Mini surveillance station in the weather proof housing box. The IP-Pro Mini comes with 500 GB of hard drive space that easily records at DVD quality. The video camera was installed about ten days after the strain gages. The following steps describe the video installation.

1. The video camera was attached to a mount.
2. The camera mount was placed on a pole near the ferry ramp which contained the strain gages. The camera is ideally faced to detect motion from the ferry boats docking to the bridge.

3. Cabling from the video camera was run to the video camera data system placed inside the weather resistant box.
4. The video camera IP-Pro Mini surveillance system was connected to the data acquisition box so when strain gages readings were recorded it would signal the camera to record surveillance.
5. All data systems were double checked to ensure everything was running properly and data was being recorded along with video surveillance.

Figure 9 is a picture of the video camera installed at the ferry ramp site. The weather proof box used to protect the data collecting system, shown in Figure 10.

Figure 9 A video camera installed and aimed at the ferry ramp

Figure 10 The data collection system installed in a water tight cabinet

2.3 Data Reduction

Through remote desktop access, data was sorted and assembled using various computer programs, including MATLAB, Mathematica, and Microsoft Excel. The data was recorded along with video footage on the laptop computer in Port Aransas, Texas. With MATLAB, a constant had to be determined to convert the voltage readings to strain. Appendix A contains the MATLAB code written to find the conversion factor. Through the use of the equation derived from the Wheatstone bridge, equation 8, and taking the derivative with respect to strain, a conversion factor of -0.076 was found.

$$\varepsilon = -0.076\mathrm{V_{ac}} \tag{9}$$

The research team programmed data reduction algorithms in Mathematica to convert voltage to force as well as find peak values. The voltage readings that come from the strain gages are converted to force by an equation that converts voltage to strain, strain to stress, and then stress to force. The constant used to convert voltage to strain was -0.076 determined in MATLAB then strain is multiplied by the modulus of elasticity of the steel stringers 30,000 ksi to convert to stress. The stress is multiplied by the stringer cross-sectional area of 17 in^2 to obtain force in kips. Nearly 100 files are recorded daily. Local peak and valley forces are compiled automatically and sent to an Excel spreadsheet. The Mathematica program performed this procedure. Forces greater than 3 kips were sorted in excel because forces smaller than 3 kips are less of a concern than the much larger forces. Using this threshold also omits values that can come from other redundant factors.

CHAPTER III

RESULTS

The converted force values are plotted using a cumulative distribution function to best represent the data. The forces are plotted along the x-axis versus the probability ranking. The CDF graphs demonstrate the raw data and shifted data (Ang & Tang, 1975). The forces are shifted plus or minus 3 kips to allow for a smooth curve in the graph. Figures 11-21 are force values from all boat types from June 2012 to March 2013. A further break down of the data is recorded in tables found in Appendix B. The tables display the maximum forces, average forces, and standard deviation forces for each stringer.

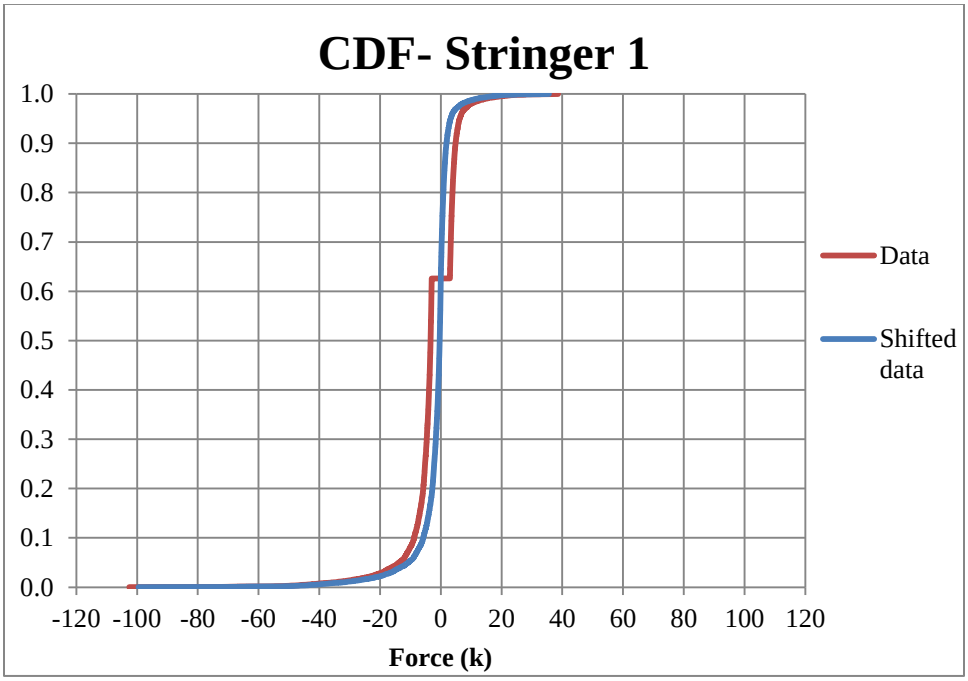

Figure 11 Cumulative Distribution of forces for stringer 1 for all boats

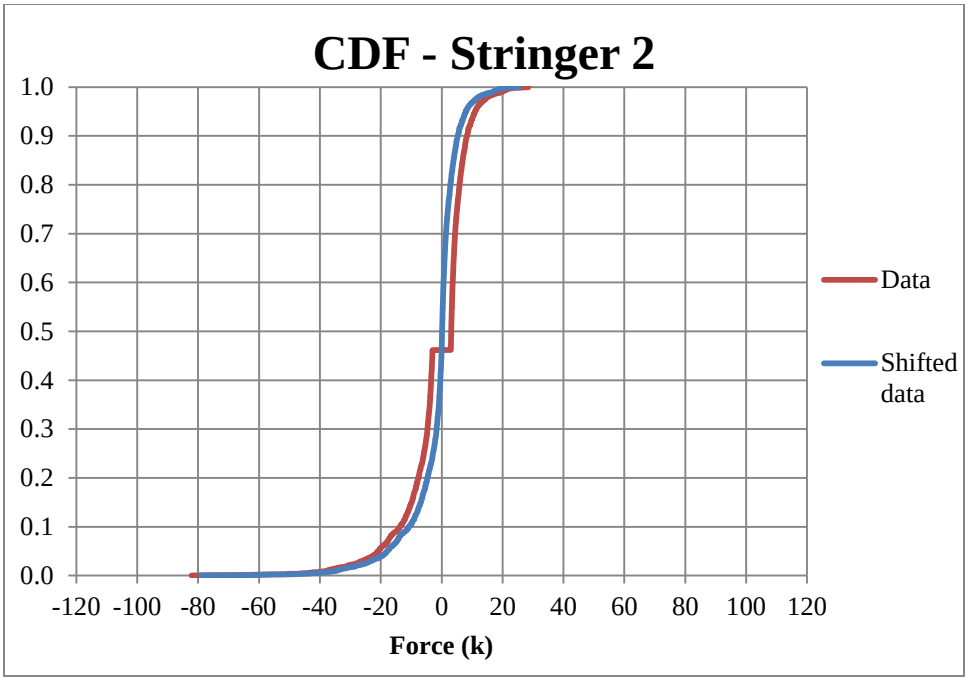

Figure 12 Cumulative Distribution of forces for stringer 2 for all boats

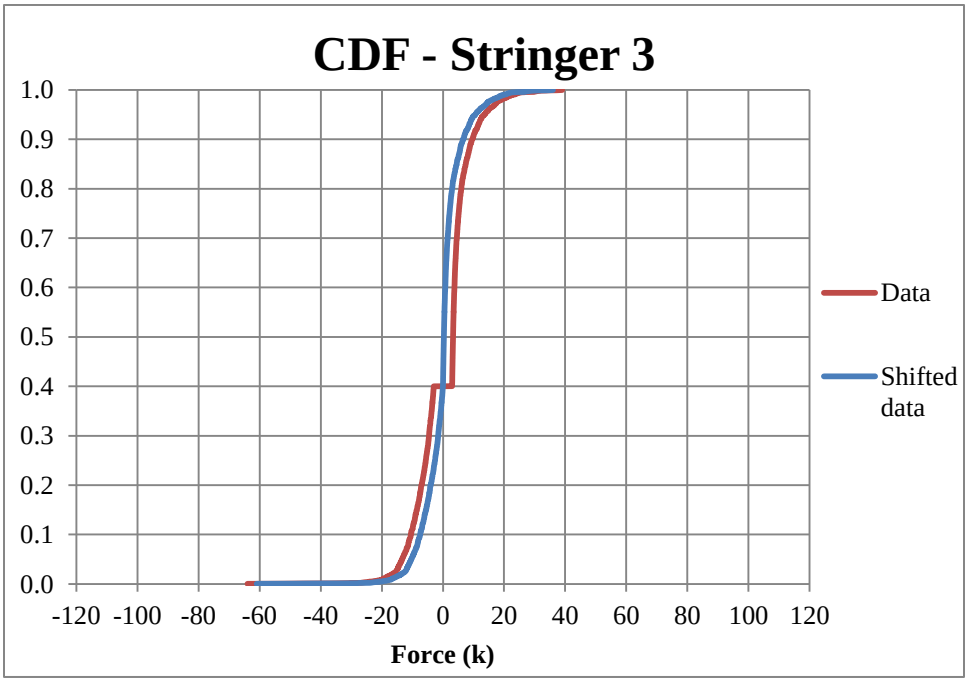

Figure 13 Cumulative Distribution of forces for stringer 3 for all boats

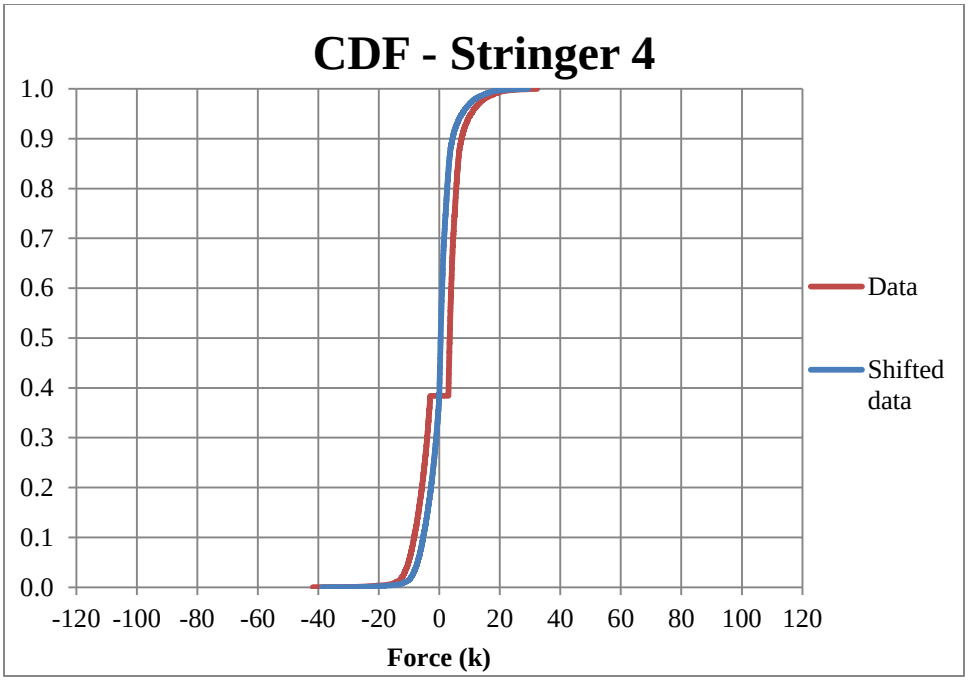

Figure 14 Cumulative Distribution of forces for stringer 4 for all boats

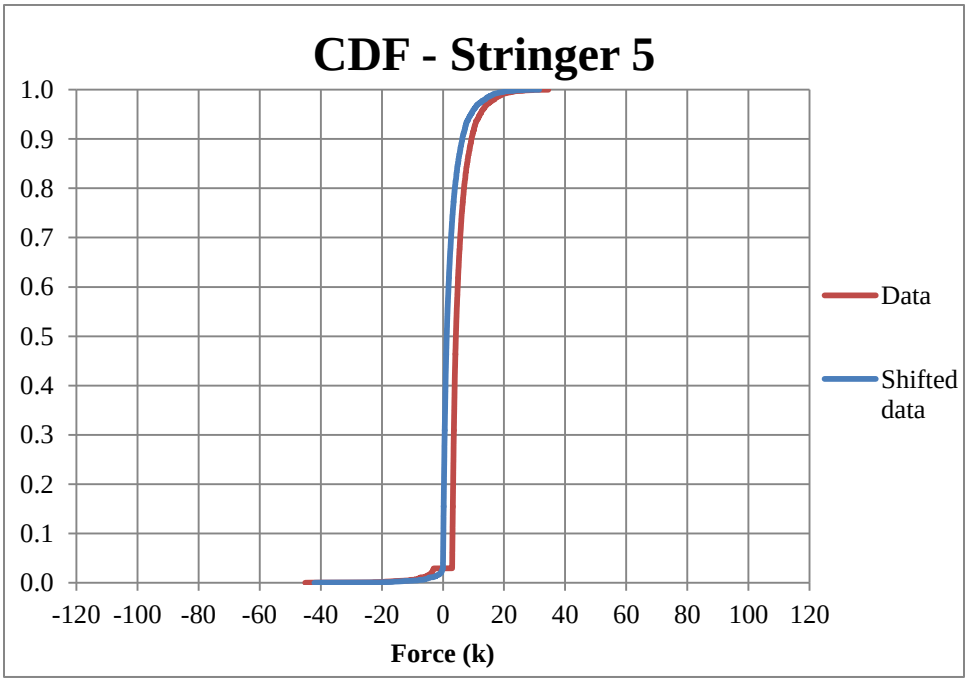

Figure 15 Cumulative Distribution of forces for stringer 5 for all boats

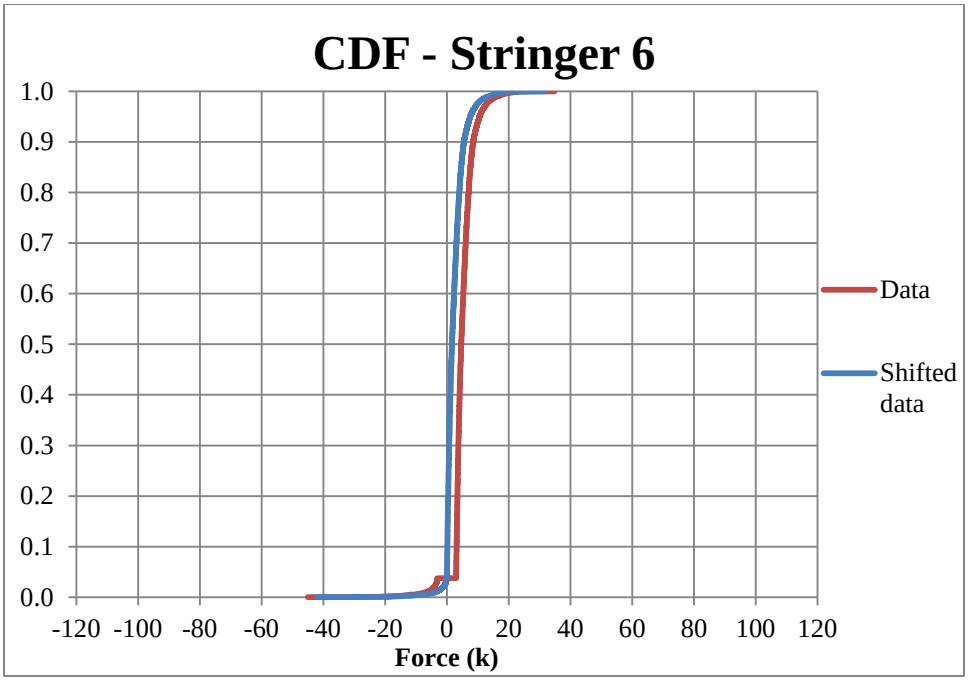

Figure 16 Cumulative Distribution of forces for stringer 6 for all boats

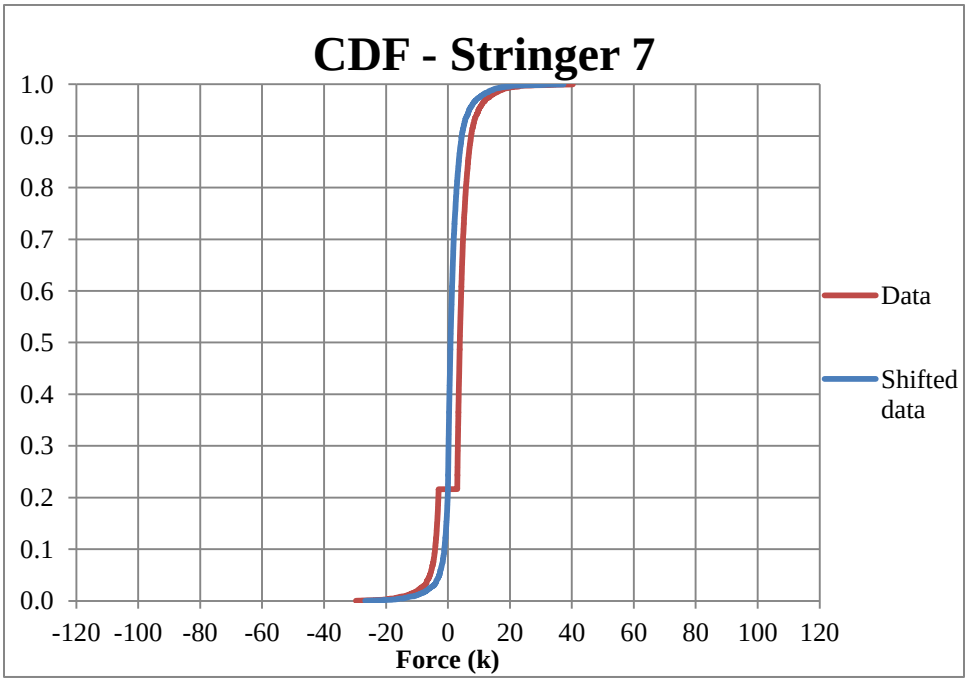

Figure 17 Cumulative Distribution of forces for stringer 7 for all boats

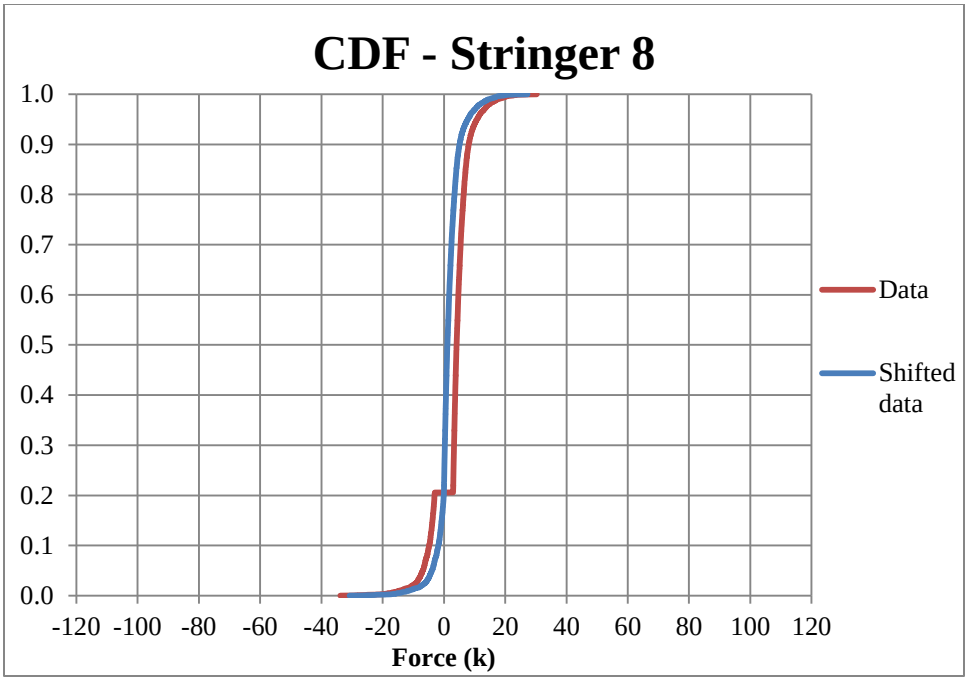

Figure 18 Cumulative Distribution of forces for stringer 8 for all boats

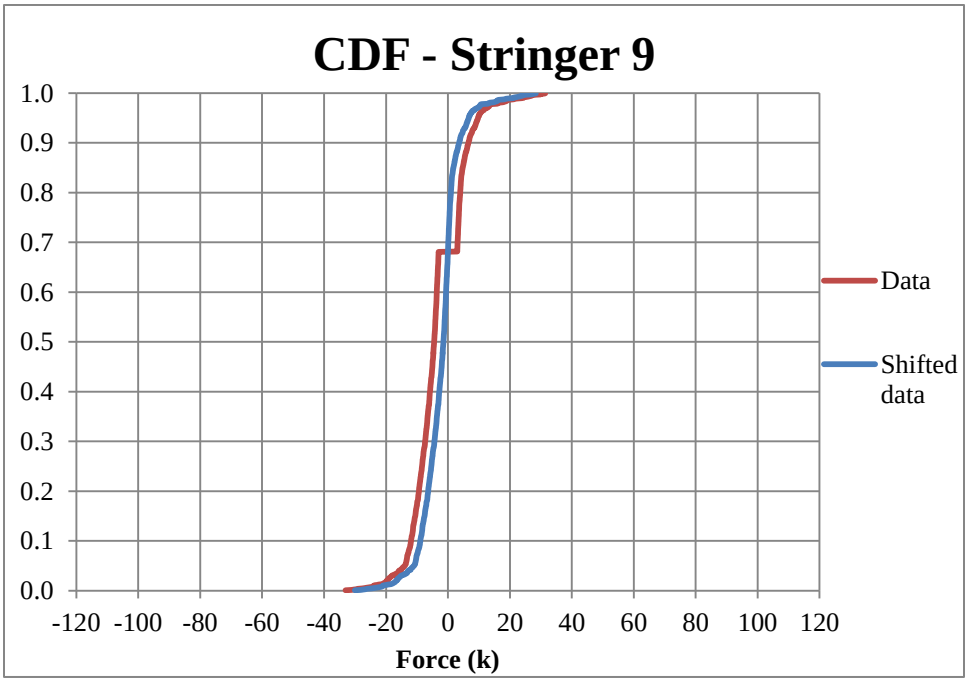

Figure 19 Cumulative Distribution of forces for stringer 9 for all boats

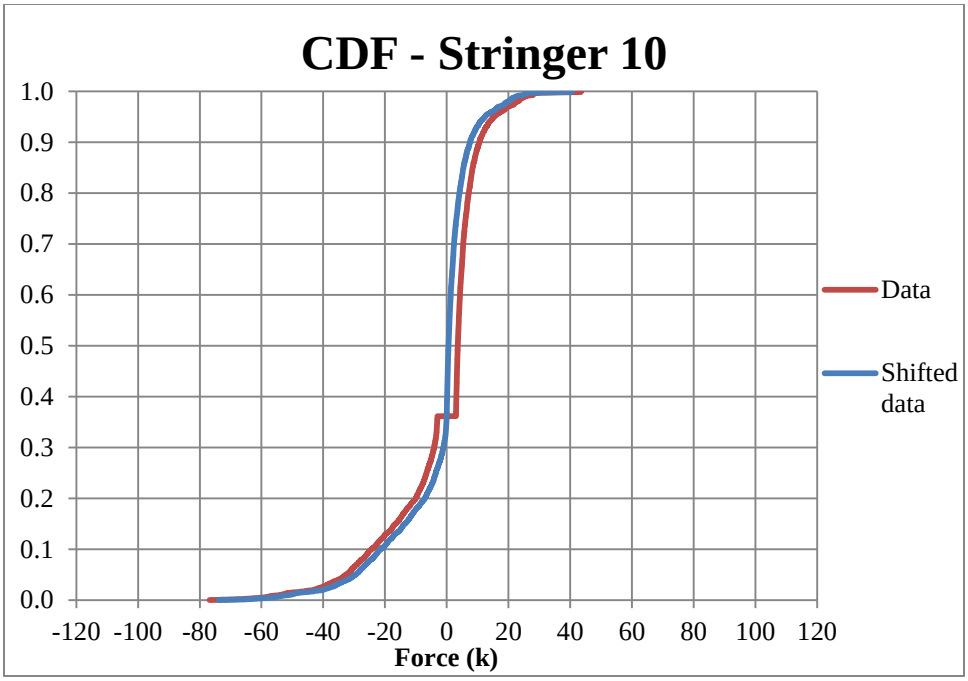

Figure 20 Cumulative Distribution of forces for stringer 10 for all boats

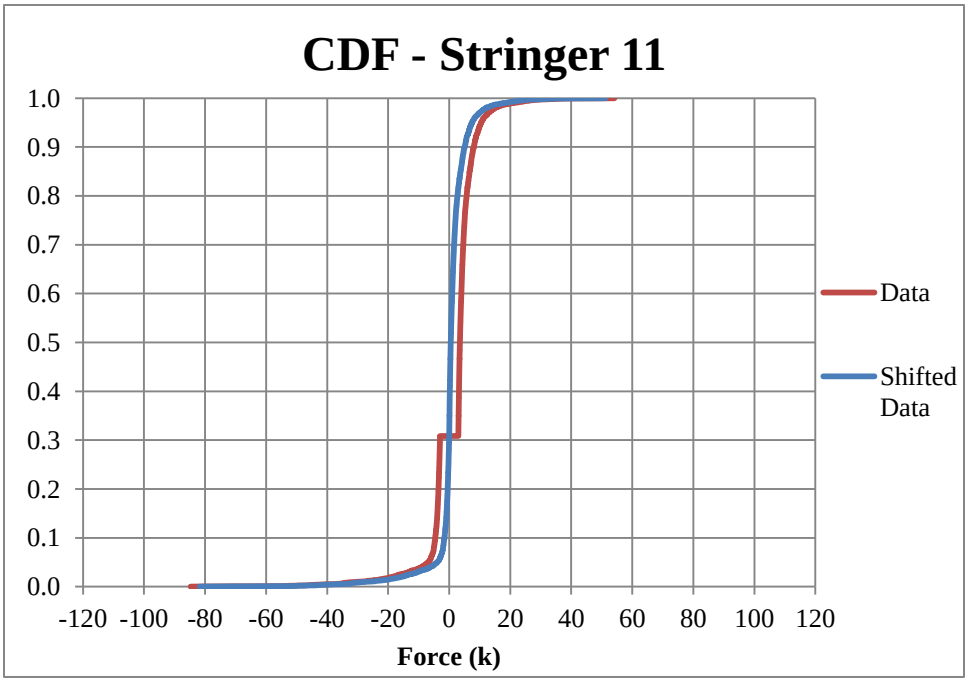

Figure 21 Cumulative Distribution of forces for stringer 11 for all boats

Bar charts were created to help visualize the different impacts happening to the bridge. Figure 22 is a bar chart of the maximum axial loads recorded in compression and tension. Figure 23 is another bar chart representing the number of load events recorded for each stringer in tension and compression. Figures 24-26 pertain to the small boats versus big boats data that was recorded for the first two months of the project; however, the video camera stopped working in August. This prevented the researchers from deciphering which type of boat caused the load event; therefore, these charts are only for the months of June and July.

A log normal distribution was used along with a cumulative distribution function to represent the compression and tension forces of each stringer. A best fit log normal distribution was used as a statistical model for the data (Hines, Montgomery, Goldsman, & Borror, 2003). These plots can be found in Appendix C for further comparison of tension and compression forces.

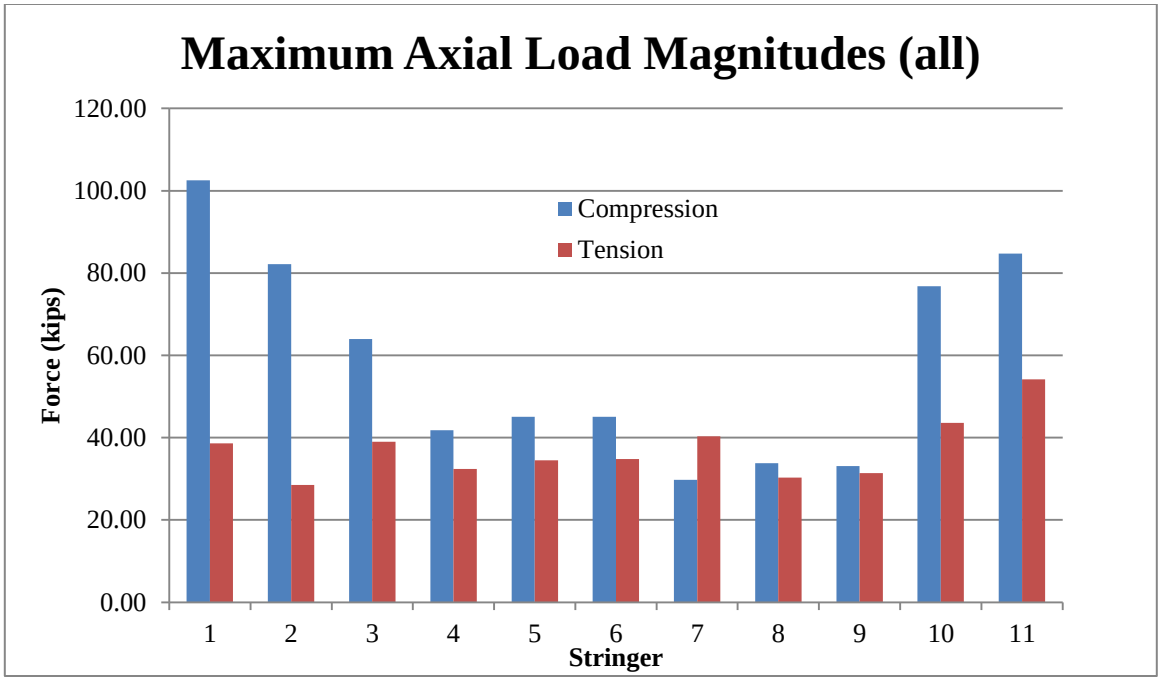

Figure 22 Bar graph of max compression and tension axial loads per stringer

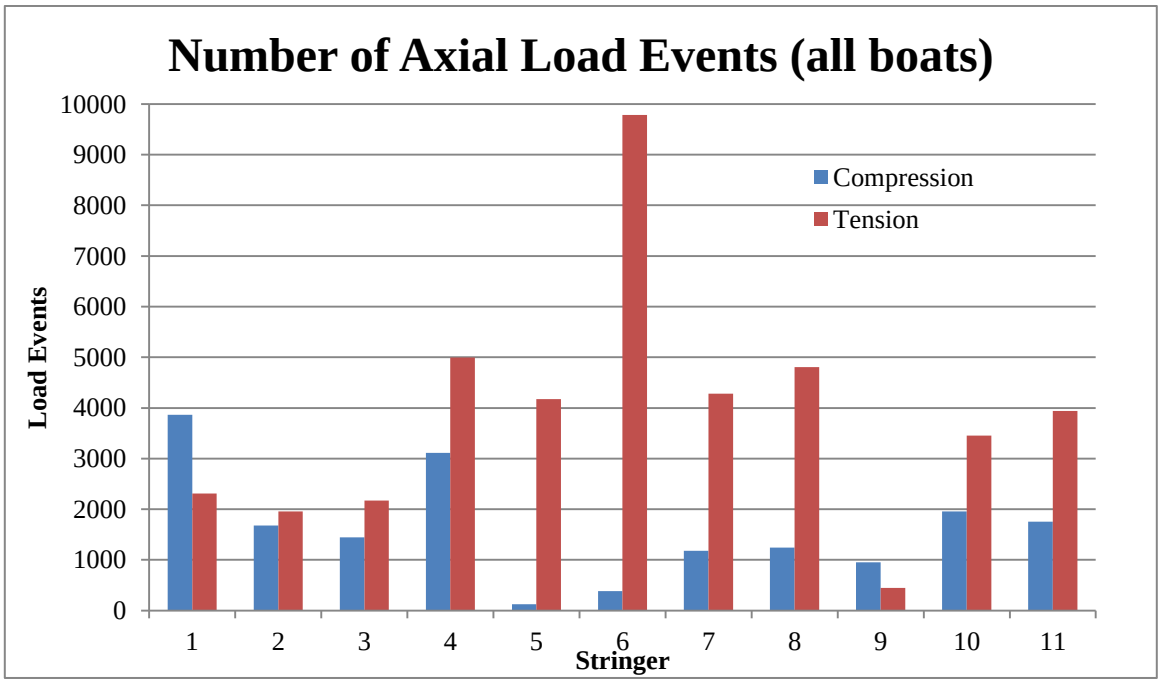

Figure 23 Number of recorded compression and tension load events per stringer

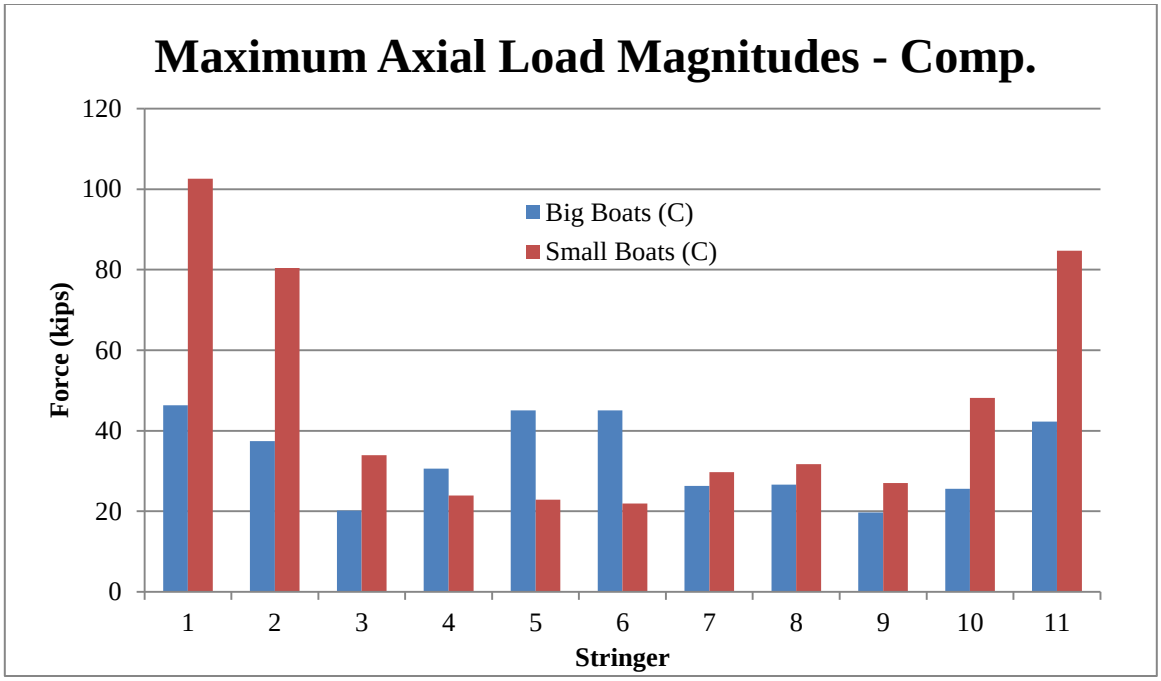

Figure 24 Maximum axial compression loads by boat size per stringer

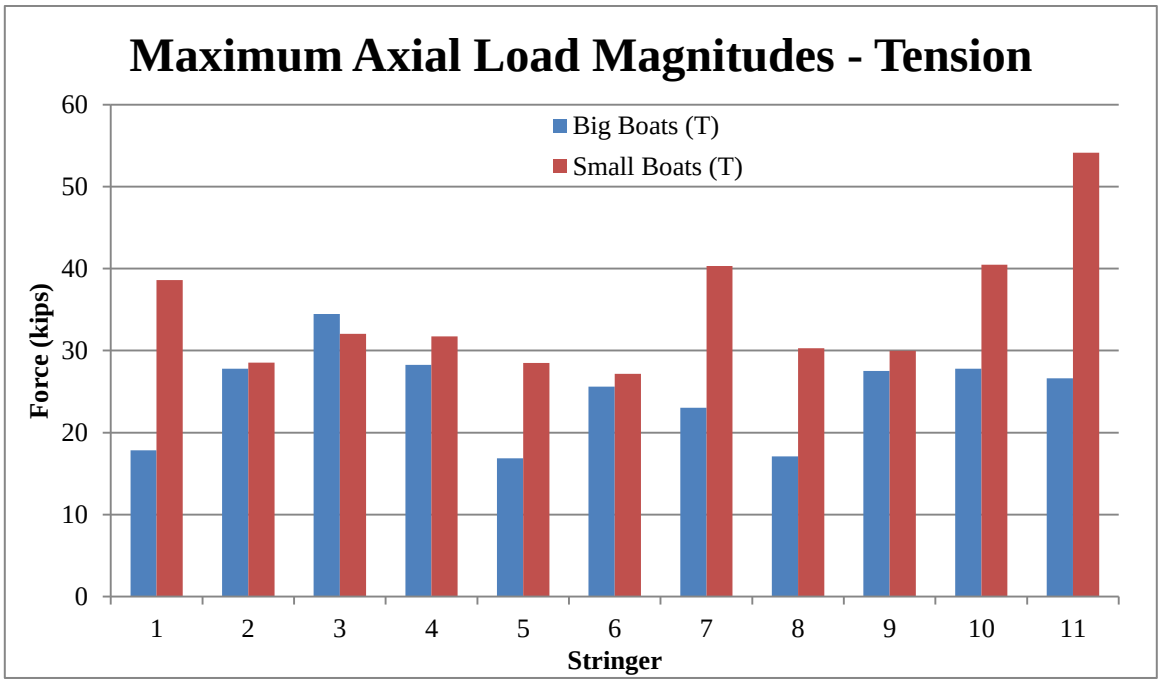

Figure 25 Maximum axial tension loads by boat size per stringer

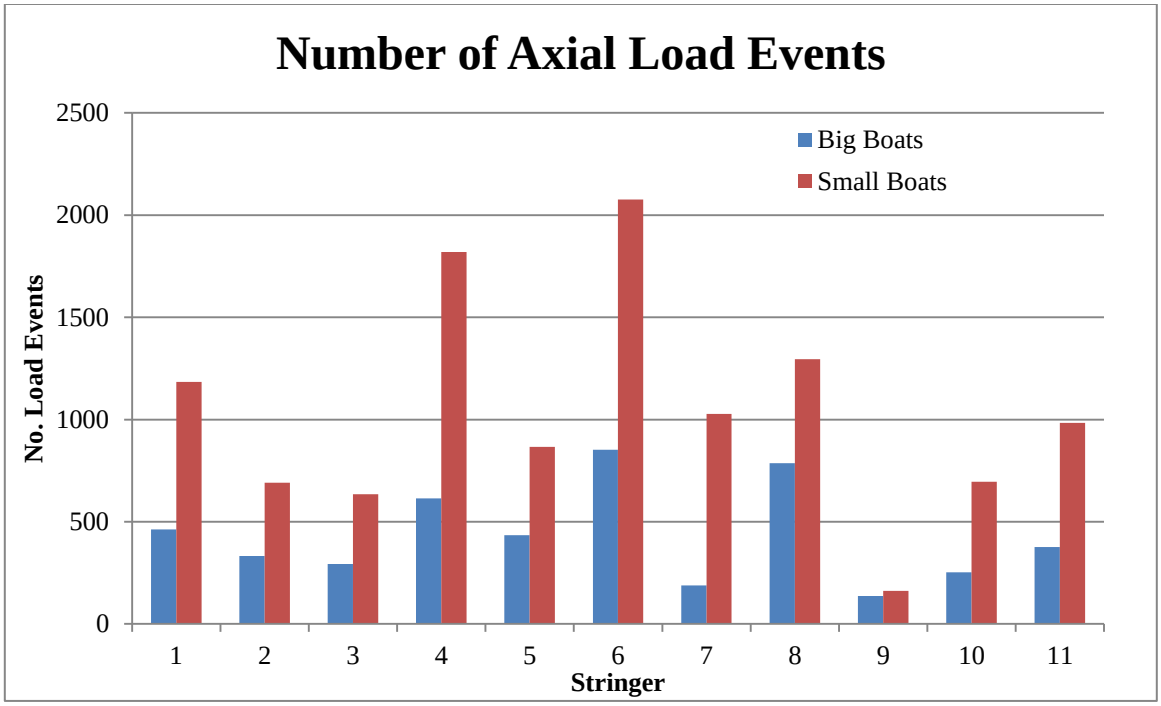

Figure 26 Number of recorded load events per stringer by boat size

CHAPTER IV

DISCUSSION

The largest recorded force values occur in outer stringers 1, 2, 10, and 11. This is evident in Figure 22 and the CDF plots. The larger forces can be attributed to a skew angle that arriving boats sometimes present upon docking. Whenever the boats accidently ram into the bridge, it usually occurs at one of the sides of the bridge. The larger forces, in majority of the stringers with the exception of stringer 7, are in compression. The ramp experiences the most force in compression when the ferry boats engage the ramp upon docking, undocking, or while attached to the ramp. The outer stringers are producing the larger loads but middle stringer 6 is recording the most load events. With stringer 6, 95% of the data recorded is in tension, hinting that the recorded force values for stringer 6 are not coming from the boat thrusting into the bridge but from other events, such as vehicles. When the cars travel across the ramp, it pulls the stringers into tension. More than likely, stringer 6 has a smaller gap within the pins located in the bearing connection, so it is pulled into tension first.

The average and standard deviation of forces are larger for compression than tension forces, shown in Table 1 and 2 in Appendix B. Compression forces are ranging from 3 kips up to 102 kips. This causes a larger spread than the tension forces which are only ranging from 3 kips to 55 kips. The number of load events for stringer 9 is much lower than the other stringers. The length of all the stringers from the headwall to the end of the bridge will not be exactly equal. Some stringers will absorb more of the loads

because the ferry boats contact those stringers first. Stringer 9 must be shorter than the stringers around it due to the lack of recorded forces.

Figure 26 illustrates more recorded data values come from small boats. The main reason for this is because smaller boats are used more often, especially at night. The small boats are also causing the larger force values because they are harder to control in rough weather and compensate more for the current. When these small boats are attempting to dock, the current causes the boats to come in at an angle and engine thrust is used to align the front of the boat. The engine thrust causes a large compression force on the side of the boat that initiated contact with the bridge.

CHAPTER V

CONCLUSION

From observing data for approximately 10 months, the largest force recorded was in stringer 1 with a value of 103 kips in compression. This gives an idea of the maximum load the ramps need to be designed to withhold. Strain measurements and video footage indicate that the docking procedure is creating the large compression forces on the ramps, especially in poor weather conditions. The outer stringers are absorbing the large forces. The bearing connections for the outer stringers need to be designed to account for this occurrence. Middle stringers 4-8 endure more tension forces than the rest of the stringers from vehicles loading onto the ferry boats. Wind and waves contribute to compression and tension by either pulling the boat away from the ramp or by pushing the boat into the ramp. As a result of the strain gage instrumentation and video footage, axial forces were accurately documented and matched to a specific boat size and load event to progress the assessment of ferry ramps in Port Aransas, Texas. It is recommended to repair and modify the bearing assemblies that connect the ferry ramp to the landing wall to accommodate the larges forces experienced by the stringers and transferred to the bearing connections. Another option is to redesign the bearing connections to something more applicable for the impact loads transpired from ferry boats.

REFERENCES

Ang, H.H-S., & Tang, W.H. (1975). *Probability Concepts in Engineering Planning and Design.* New York: John Wiley & Sons, Inc.

Federal Highway Administration (2012). *Bridge Inspector's Reference Manual* (Publication No. FHWA NHI 12-049). Washington, DC: U.S. Government Printing Office.

Federal Highway Administration (2012). *Who We Are*. Retrieved from < http://www.fhwa.dot.gov/about/ > (27 January 2015).

Federal Highway Administration (2014). *Bridge by Structure Type* (Data File). Retrieved from < http://www.fhwa.dot.gov/bridge/britab.cfm > (2 February 2015).

Hines, W.W., Montgomery, D.C., Goldsman, D.M., & Borror, C.M. (2003). *Probability and Statistics in Engineering.* United States of America: John Wiley & Sons, Inc.

Texas Department of Transportation. (2013). *Bridge Inspection Manual* (Manual Notice 2013-1). Retrieved from < http://onlinemanuals.txdot.gov/ > (5 February 2015).

APPENDIX A

CONVERSION FACTOR

The MATLAB code used for determining the conversion factor utilizing the Wheatstone bridge circuit is shown below.

```
%Conversion Factor for converting Voltage to Strain
%Note: this is for a full bridge

%ep is epsilon
syms ep
format short
Vin=10; %input voltage, volts
nu=0.29; %poisson's ratio
Fg=2.04; %gage factor
R=120;  %Resistance, ohms

%change in resistance for resistors 1-4 in Wheatstone
bridge
dR1=R*Fg*ep;
dR2=R*Fg*-nu*ep;
dR3=R*Fg*ep;
dR4=R*Fg*-nu*ep;

%initial resistance plus change in resistance
R1=R+dR1;
R2=R+dR2;
R3=R+dR3;
R4=R+dR4;

%voltage across 'ac' in Wheatstone bridge
dVac=Vin*( R4/(R1+R4) - R3/(R2+R3))

%simplify the equation in terms of ep
simplify(dVac)

%take derivative
vslope=diff(dVac)

%plug zero in for epsilon and take 1/vslope to get
conversion factor
subs(1/vslope,ep,0)
```

APPENDIX B

TABLES

It should be noted for Table 1-3 that the values recorded under big boats and small boats are only for the months of June and July because the video camera stopped recording surveillance in August. The values under all boats are cumulated from all the months of recording data in Port Aransas, TX.

Table 1 Max, average, & standard deviation forces in compression per stringer

	Compression Forces (kips)								
	All Boats			Big Boats			Small Boats		
	Max.	x-bar	σ_{n-1}	Max.	x-bar	σ_{n-1}	Max.	x-bar	σ_{n-1}
Stringer 1	102.56	6.80	7.26	46.29	8.03	8.81	102.56	7.10	8.52
Stringer 2	82.13	10.06	9.41	37.39	13.81	9.64	80.40	11.42	13.29
Stringer 3	63.97	8.18	4.98	20.16	9.41	3.93	33.91	8.68	4.93
Stringer 4	41.80	6.73	3.40	30.60	6.46	3.44	23.94	6.87	3.20
Stringer 5	45.08	7.81	7.10	45.08	20.33	18.64	22.92	6.53	4.16
Stringer 6	45.03	6.54	5.67	45.03	10.95	13.73	21.95	7.71	5.15
Stringer 7	29.72	5.38	3.67	26.31	5.90	5.65	29.72	6.61	4.89
Stringer 8	33.82	6.05	3.91	26.59	5.96	2.73	31.71	6.56	4.36
Stringer 9	33.06	7.86	4.59	19.68	8.86	3.39	27.04	8.49	5.17
Stringer 10	76.82	17.13	14.28	25.57	11.49	6.71	48.14	12.14	11.29
Stringer 11	84.74	6.56	8.26	42.30	7.82	8.11	84.74	8.90	13.46

Table 2 Max, average, & standard deviation forces in tension per stringer

	Tension Forces (kips)								
	All Boats			Big Boats			Small Boats		
	Max.	x-bar	σ_{n-1}	Max.	x-bar	σ_{n-1}	Max.	x-bar	σ_{n-1}
Stringer 1	38.60	4.92	3.33	17.83	5.28	2.66	38.60	5.61	5.66
Stringer 2	28.51	6.13	3.76	27.81	6.69	4.54	28.51	6.16	3.95
Stringer 3	39.02	6.46	4.80	34.46	8.09	6.80	32.06	6.79	5.06
Stringer 4	32.37	5.66	3.45	28.25	6.32	4.10	31.72	5.37	3.18
Stringer 5	34.49	5.56	3.37	16.86	4.60	2.04	28.50	5.75	3.83
Stringer 6	34.81	5.58	2.73	25.60	5.62	3.02	27.15	5.50	2.60
Stringer 7	40.32	5.31	3.19	23.01	5.52	3.18	40.32	5.67	4.10
Stringer 8	30.29	5.65	3.07	17.11	5.10	1.95	30.29	5.89	3.47
Stringer 9	31.40	6.64	5.17	27.50	9.23	6.39	29.97	9.37	7.43
Stringer 10	43.62	7.11	5.42	27.77	7.77	5.58	40.48	6.45	4.50
Stringer 11	54.14	5.61	3.96	26.62	6.13	4.25	54.14	5.82	4.88

Table 3 Number of recorded axial load events by boat size and stringer

	Axial Load Events								
	All Boats			Big Boats			Small Boats		
	Comp.	Ten.	Total	Comp.	Ten.	Total	Comp.	Ten.	Total
Stringer 1	3866	2310	6176	290	172	462	918	266	1184
Stringer 2	1676	1954	3630	74	258	332	223	468	691
Stringer 3	1448	2171	3619	113	181	294	368	266	634
Stringer 4	3112	4994	8106	204	410	614	828	992	1820
Stringer 5	126	4172	4298	6	428	434	33	833	866
Stringer 6	381	9782	10163	15	837	852	97	1979	2076
Stringer 7	1180	4279	5459	27	161	188	234	794	1028
Stringer 8	1245	4806	6051	122	665	787	414	882	1296
Stringer 9	949	444	1393	60	76	136	123	39	162
Stringer 10	1955	3453	5408	51	201	252	128	567	695
Stringer 11	1756	3938	5694	119	257	376	232	751	983

APPENDIX C

ADDITIONAL FIGURES

For each of the eleven stringers, a compression and tension plot was generated from the data. The forces are plotted using a log normal distribution function along with a cumulative distribution function to represent the compression and tension forces of each stringer. To simplify comparing the tension and compression forces, the figures begin on the following page to allow fitting the two plots for each stringer on the same page.

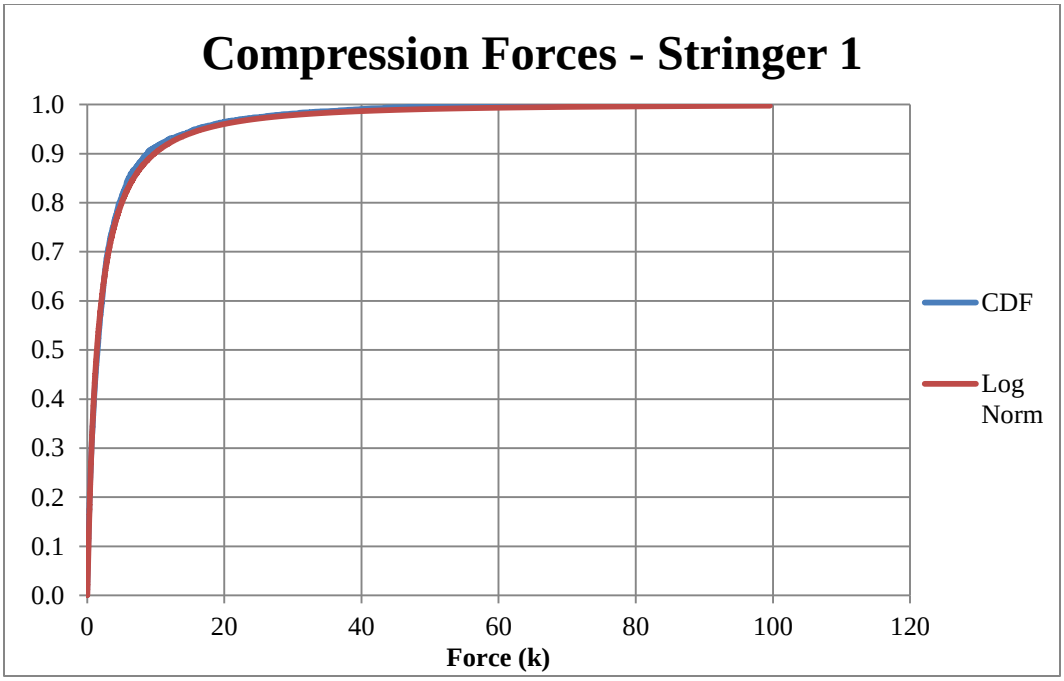

Figure 27 Stringer 1 compression forces

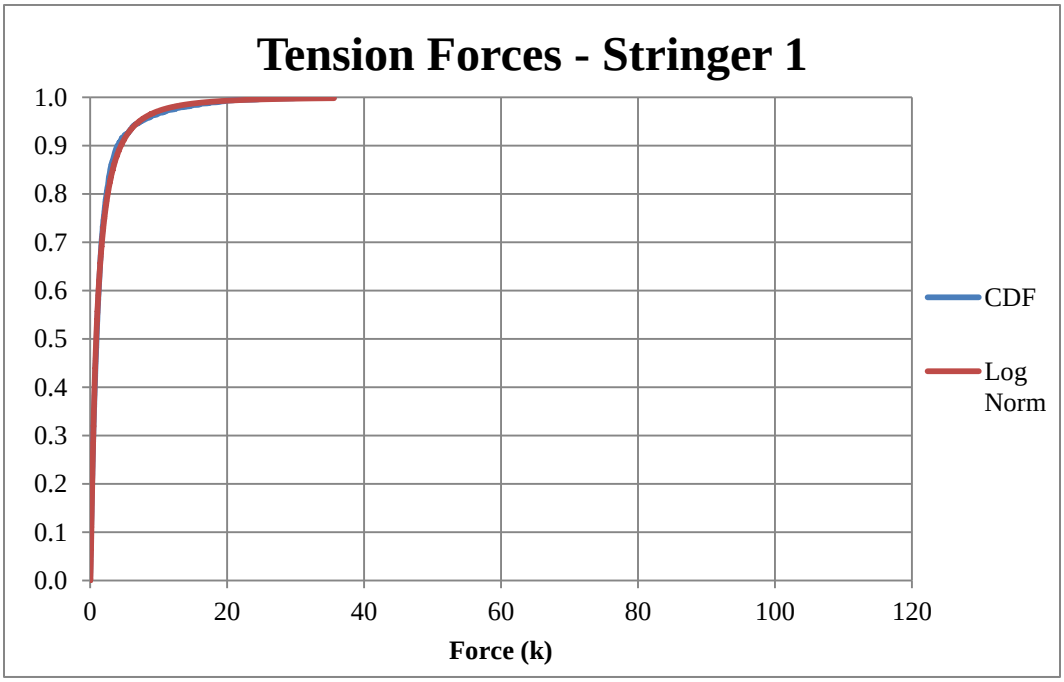

Figure 28 Stringer 1 tension forces

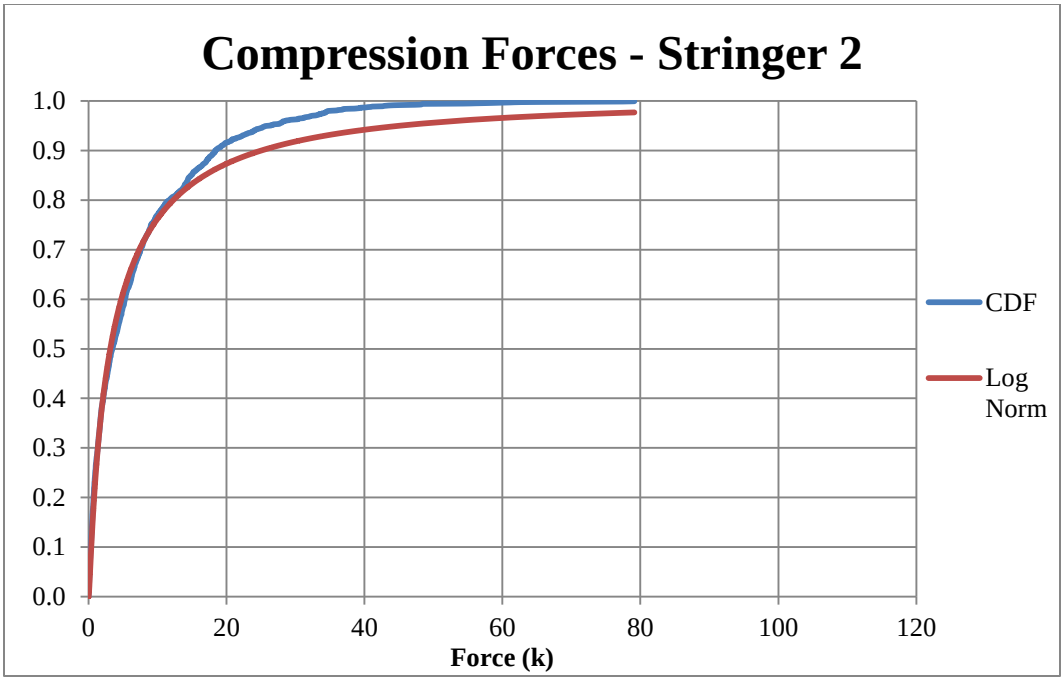

Figure 29 Stringer 2 compression forces

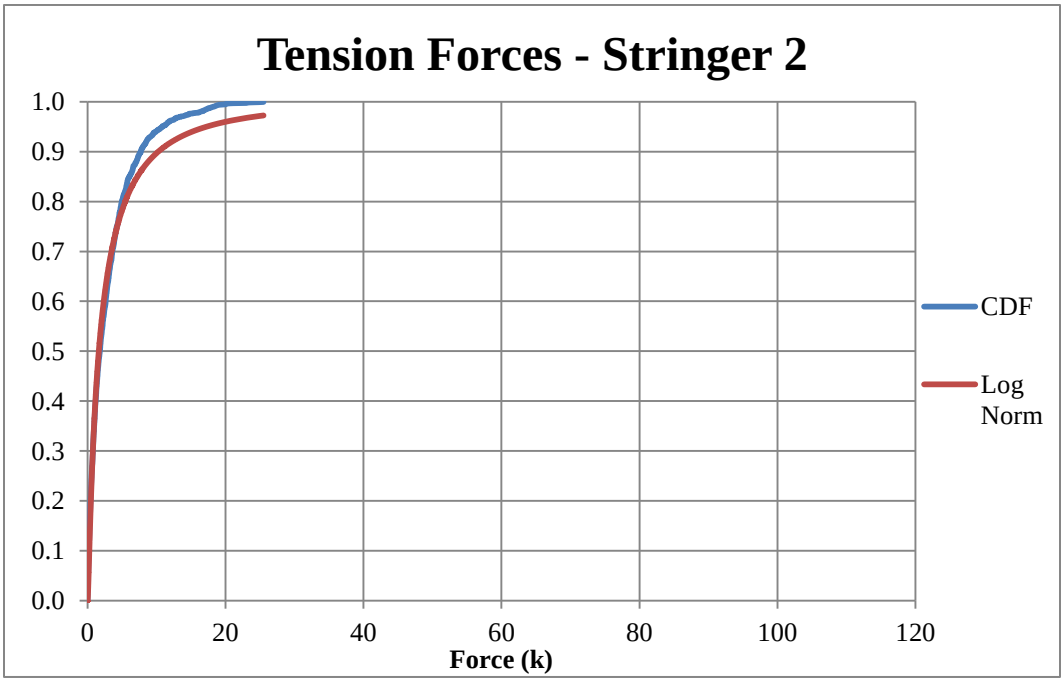

Figure 30 Stringer 2 tension forces

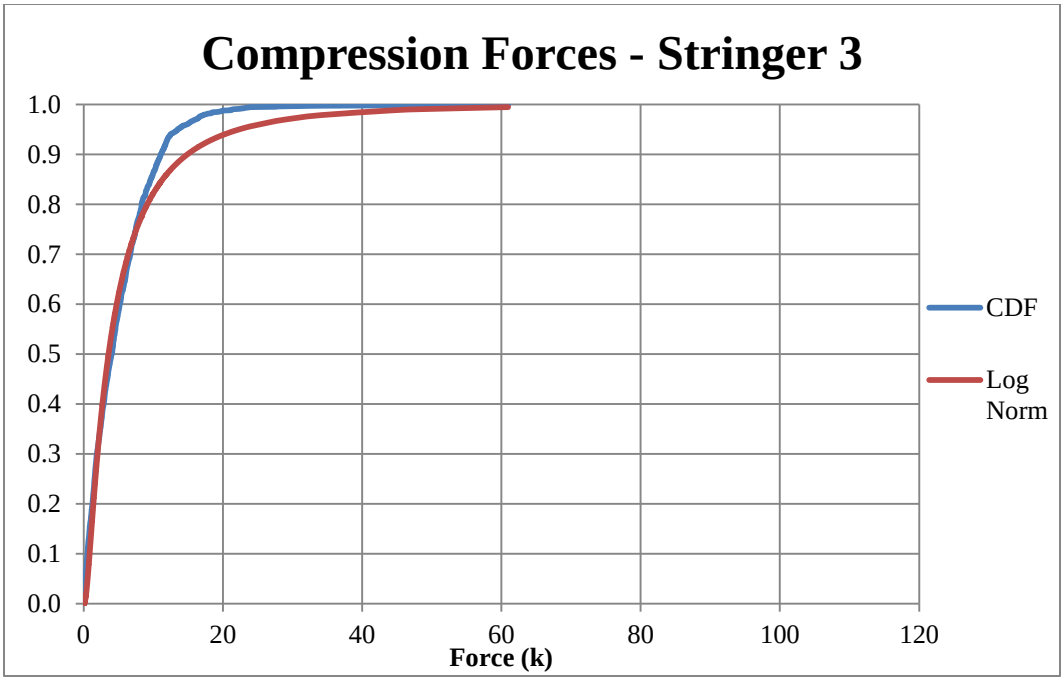

Figure 31 Stringer 3 compression forces

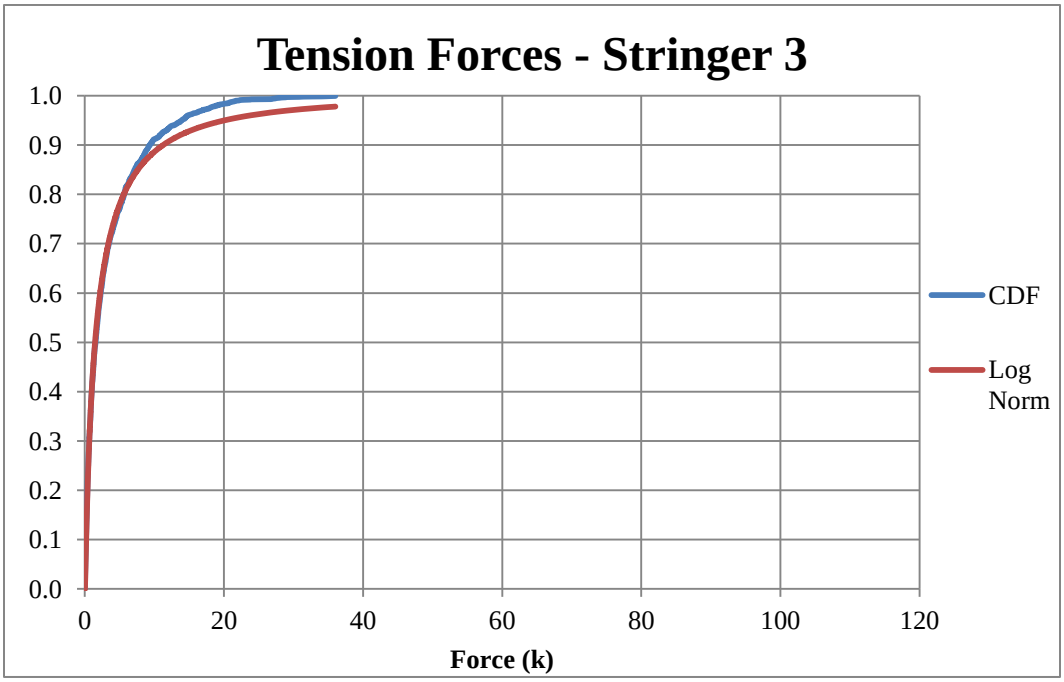

Figure 32 Stringer 3 tension forces

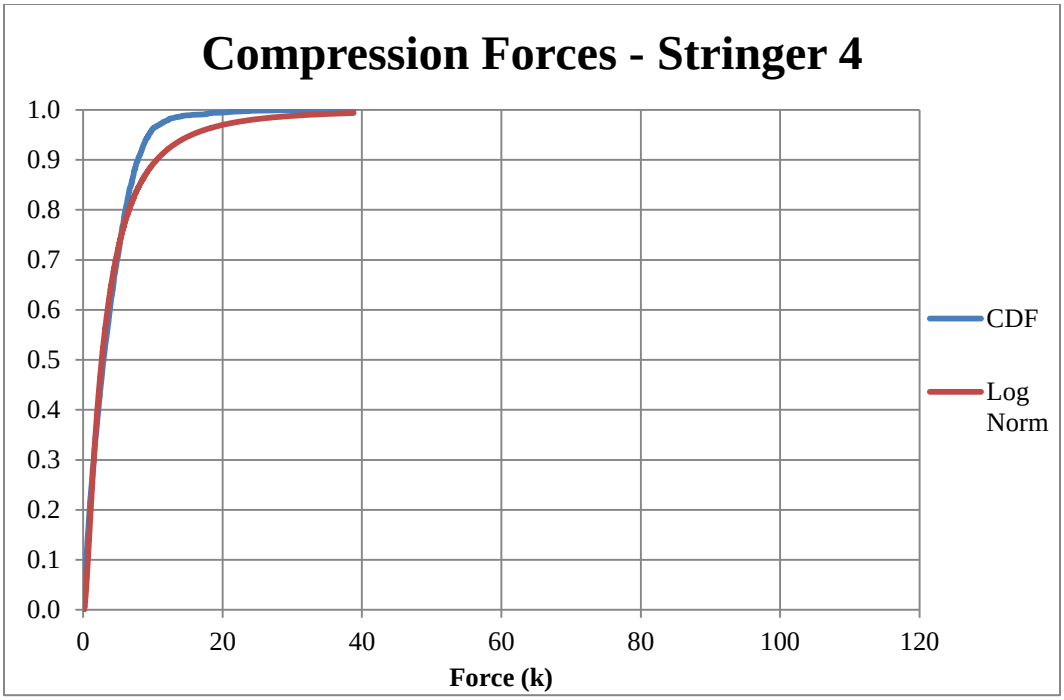

Figure 33 Stringer 4 compression forces

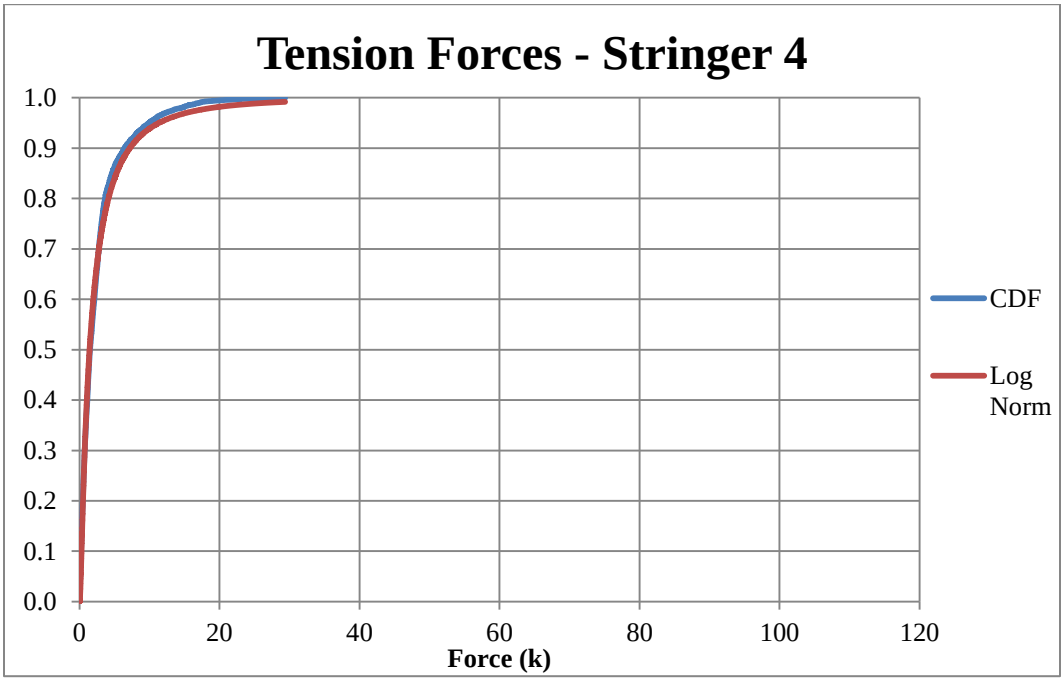

Figure 34 Stringer 4 tension forces

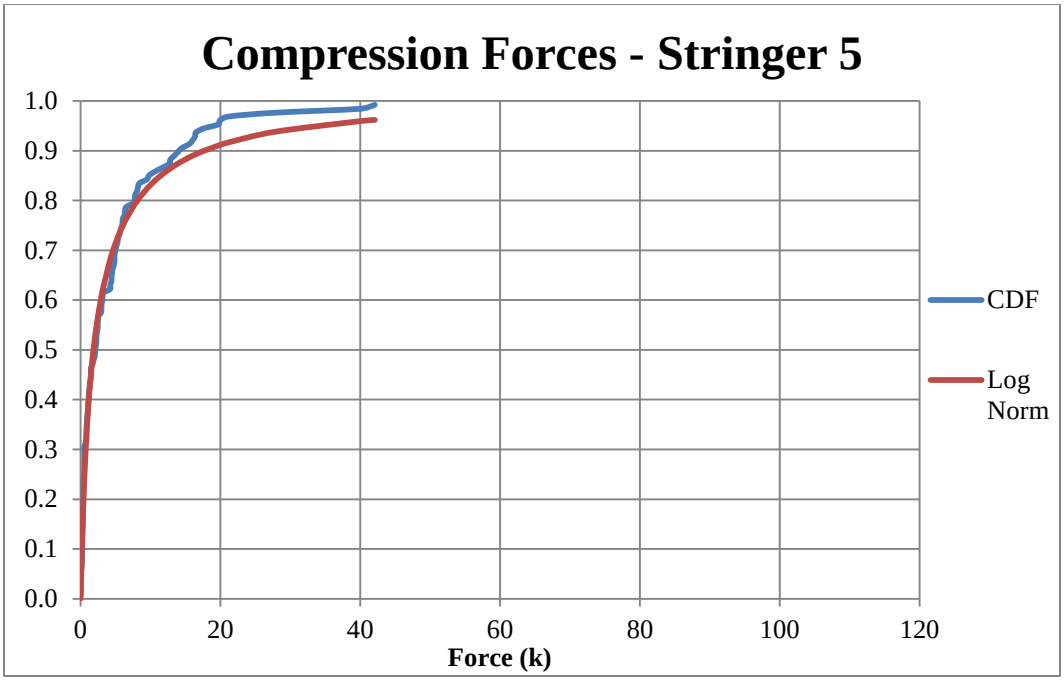

Figure 35 Stringer 5 compression forces

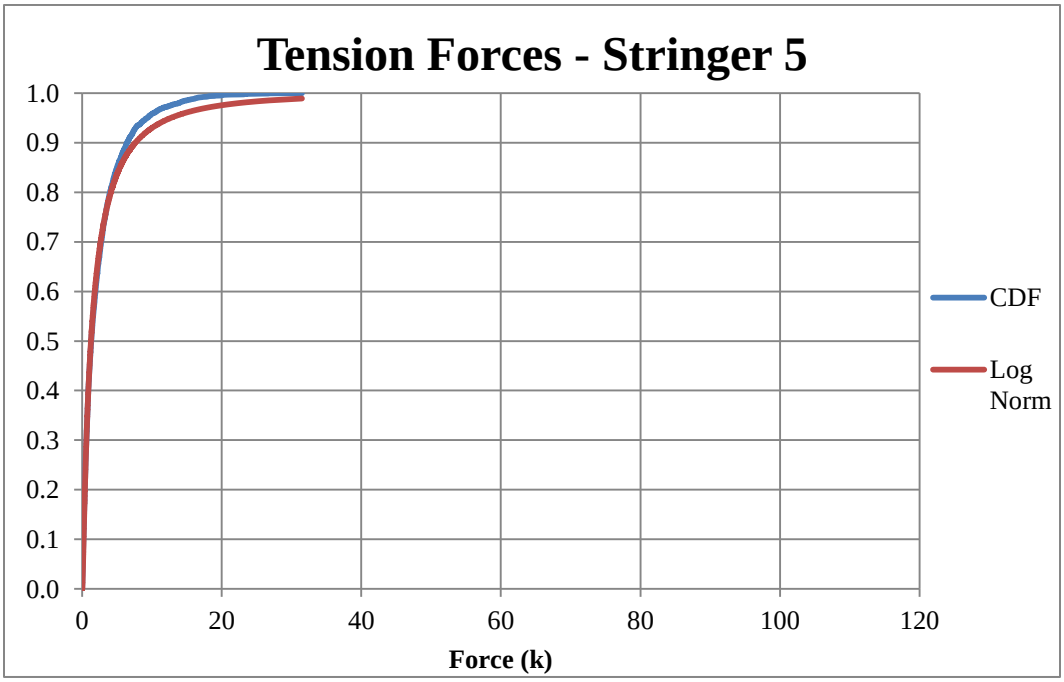

Figure 36 Stringer 5 tension forces

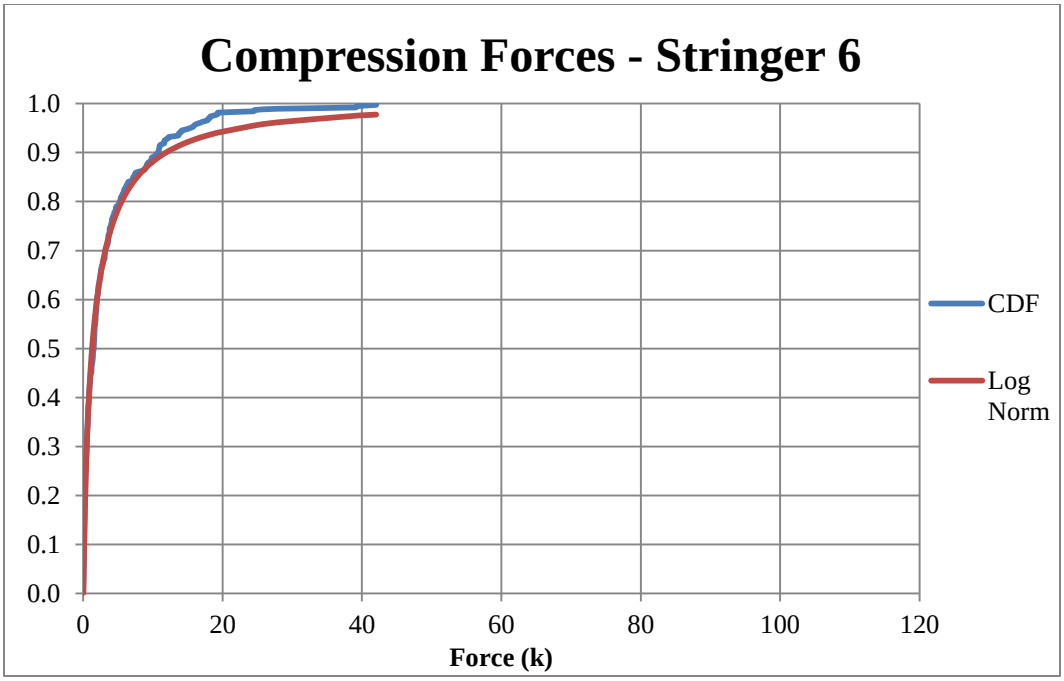

Figure 37 Stringer 6 compression forces

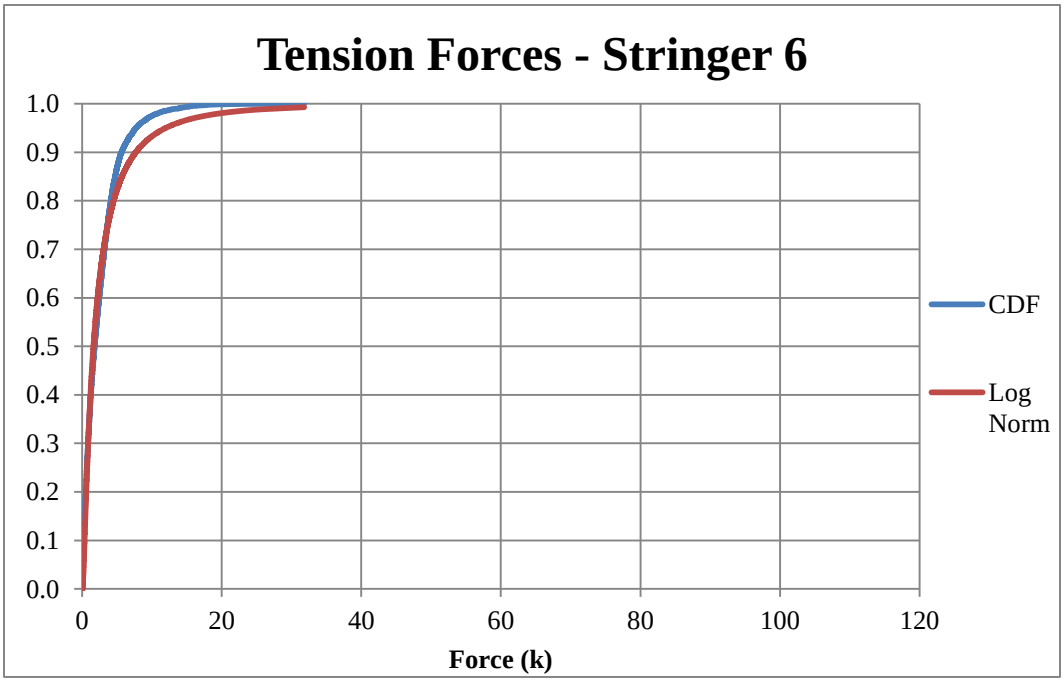

Figure 38 Stringer 6 tension forces

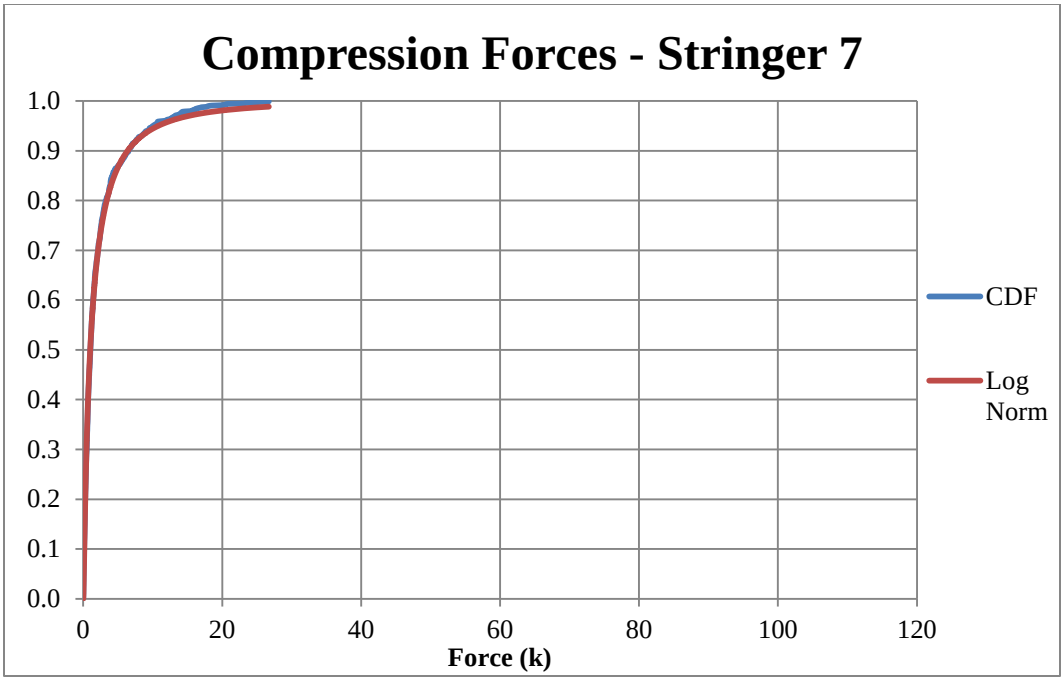

Figure 39 Stringer 7 compression forces

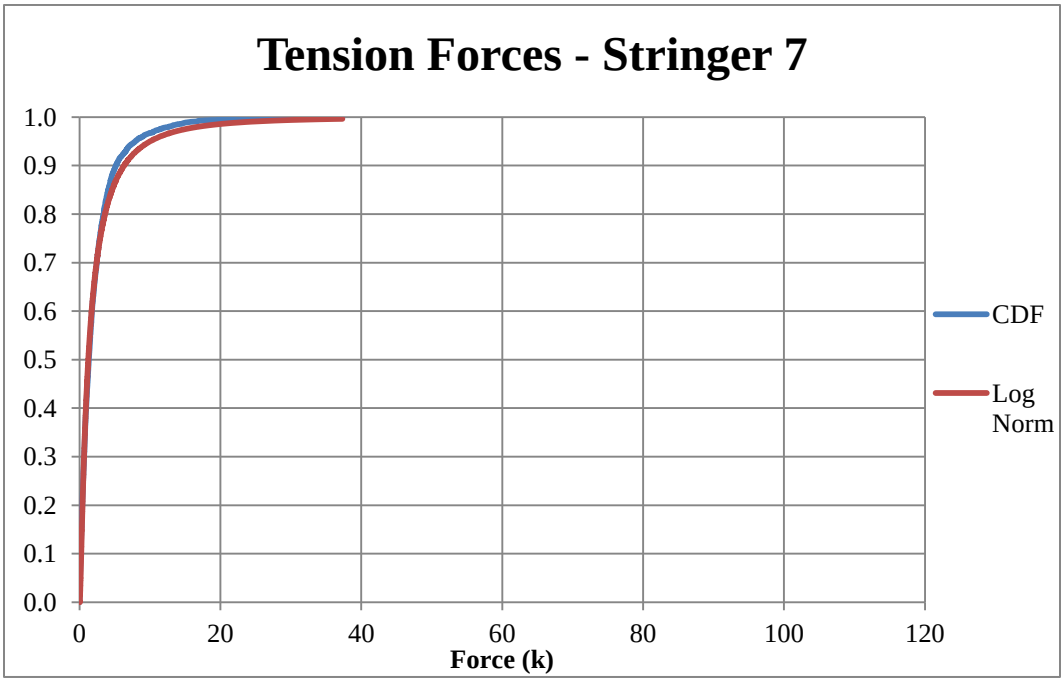

Figure 40 Stringer 7 tension forces

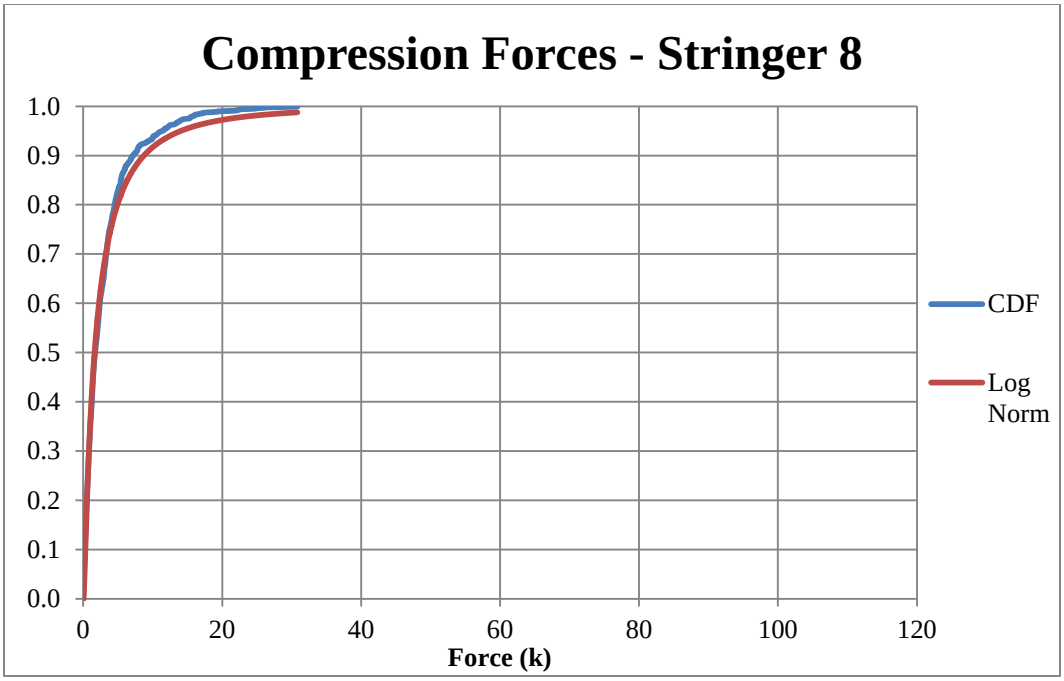

Figure 41 Stringer 8 compression forces

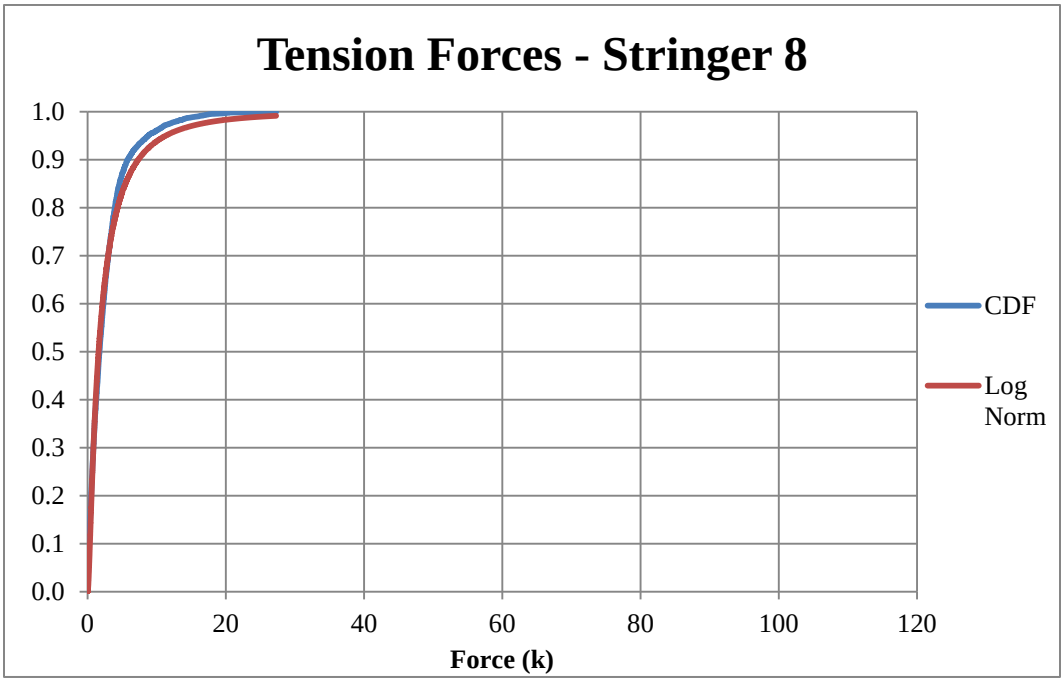

Figure 42 Stringer 8 tension forces

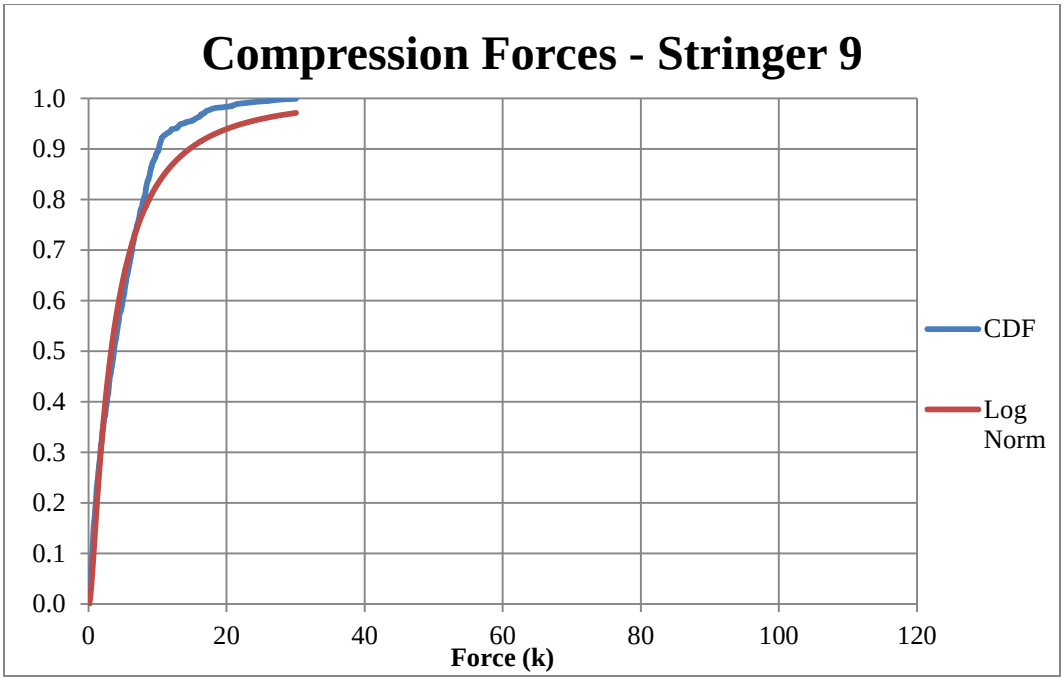

Figure 43 Stringer 9 compression forces

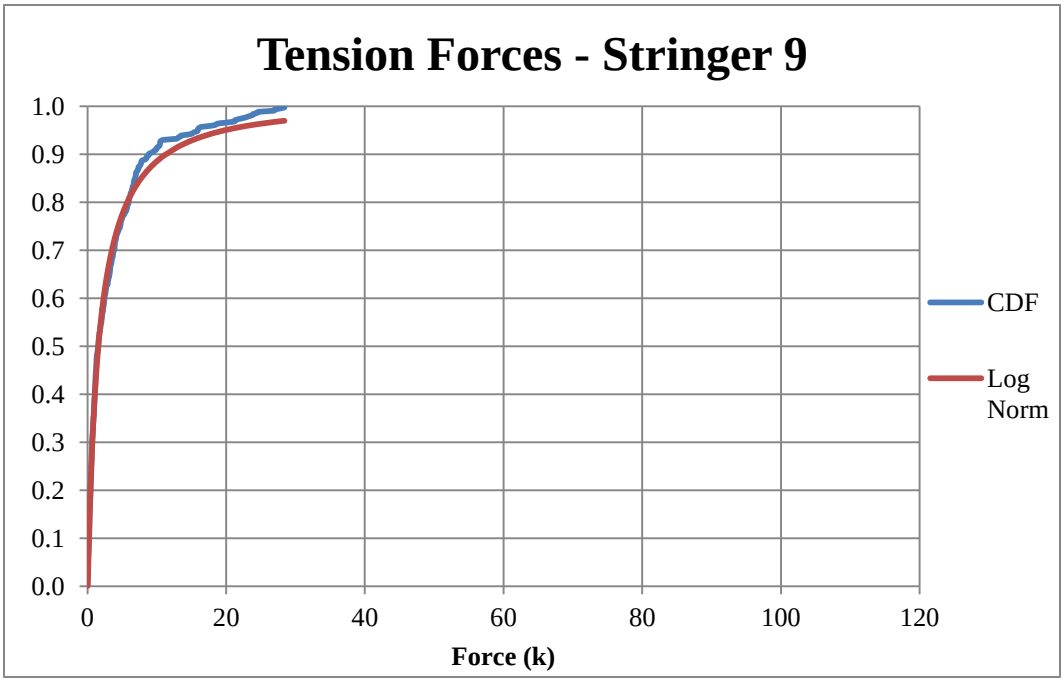

Figure 44 Stringer 9 tension forces

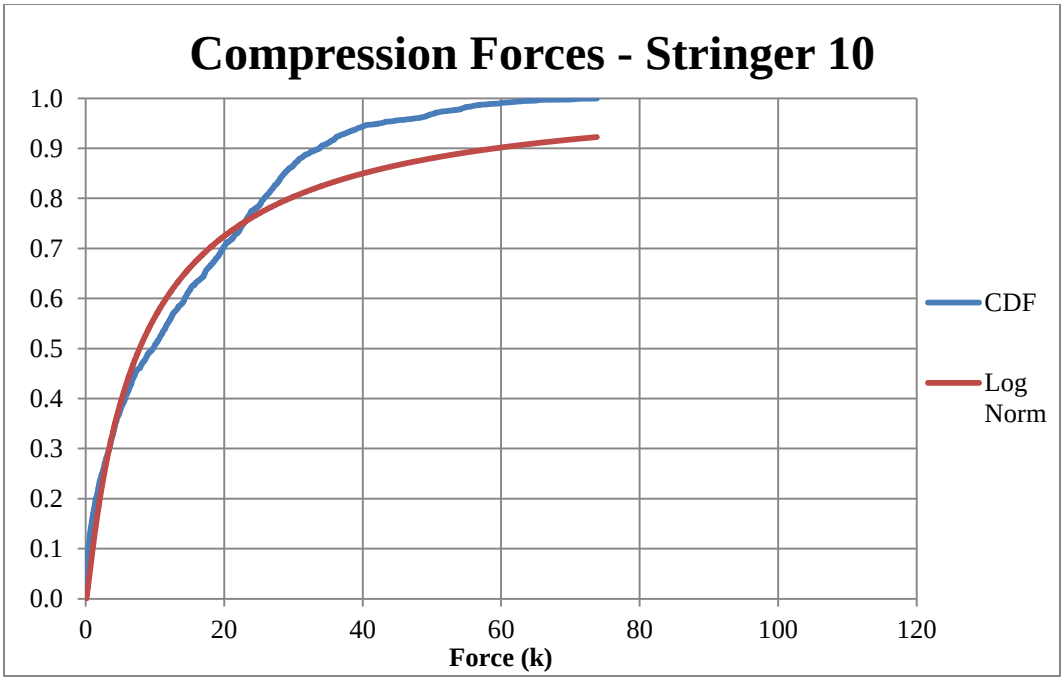

Figure 45 Stringer 10 compression forces

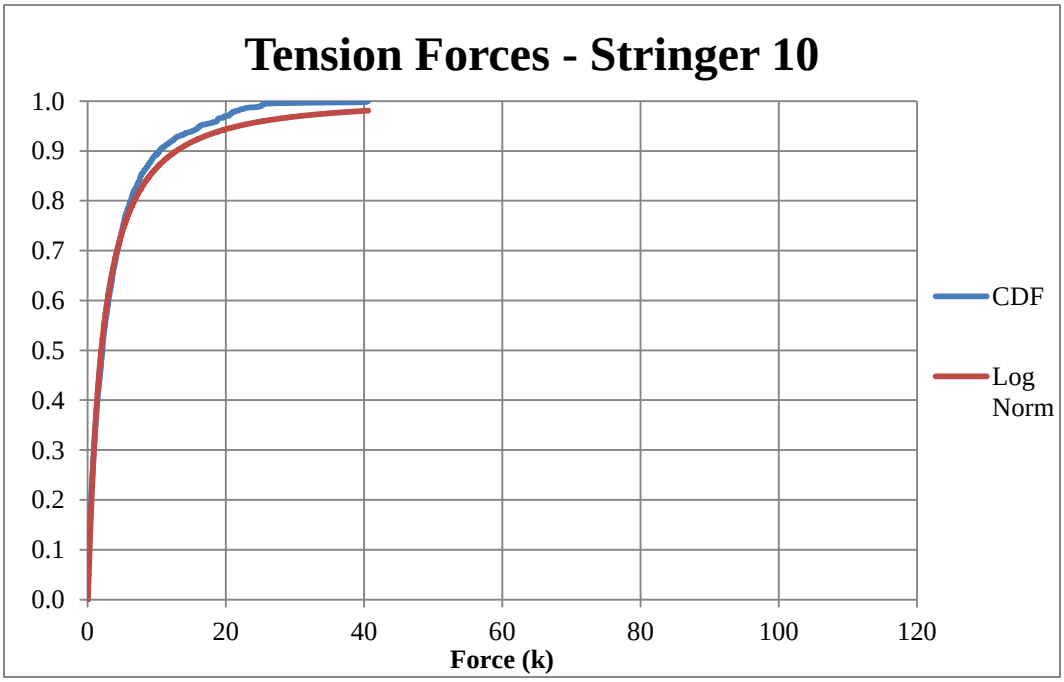

Figure 46 Stringer 10 tension forces

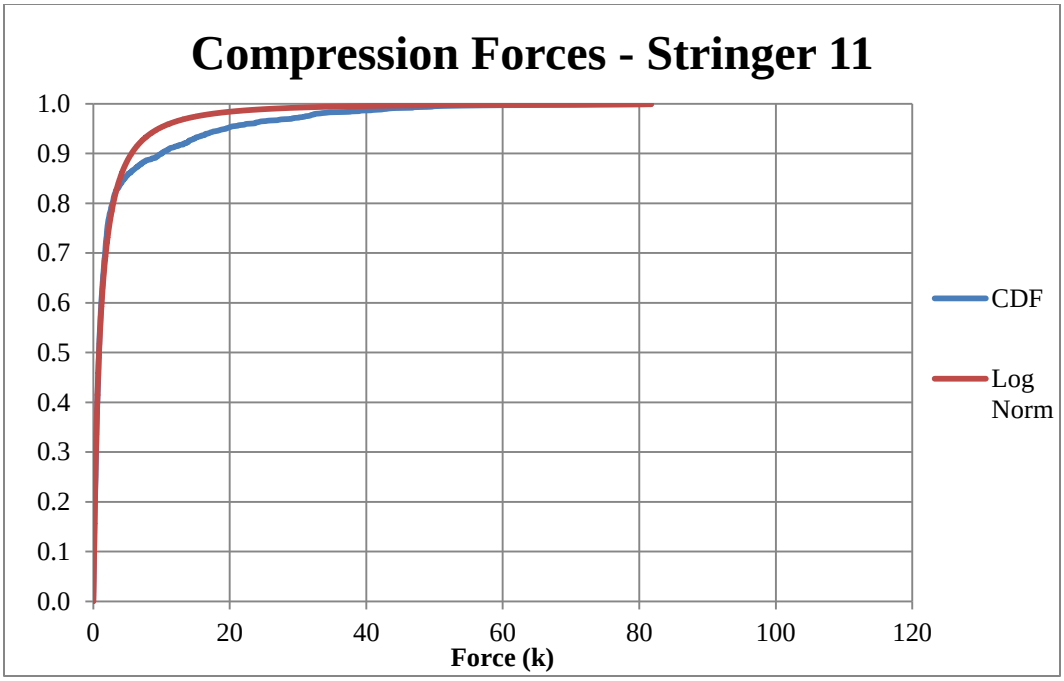

Figure 47 Stringer 11 compression forces

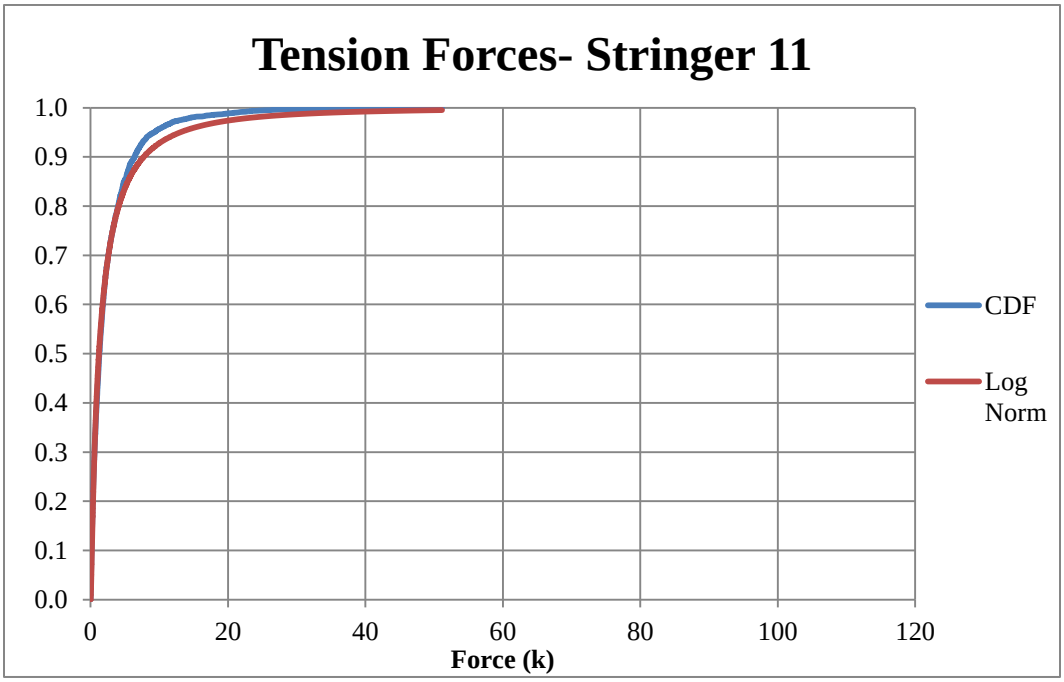

Figure 48 Stringer 11 tension forces